Special Issue on
Nuclear Science and Technology

ARTICLE

Characterization of tailings and low-grade ore from small-scale gold mining (SSGM) in Paracale, Camarines Norte and from large-scale gold mining (LSGM) in Aroroy, Masbate: Assessing environmental risks and sustainability for future green lixiviant applications

John Henry C. Gervasio*[1], Alexandria M. Tanciongco[1,2], Rico Neil M. Quierrez[1], Jessa Mae V. Estoque[1], Katrina Mae S. Flores[1], Angel T. Bautista VII[1], Cris Reven L. Gibaga[1,2,3], and Jessie O. Samaniego[1]

[1]Department of Science and Technology - Philippine Nuclear Research Institute (DOST-PNRI), Commonwealth Avenue, Diliman, Quezon City, 1101 Philippines
[2]University of Leicester, University Road, Leicester, LE1 7RH United Kingdom
[3]British Geological Survey, Keyworth, Nottingham, NG12 5GG United Kingdom

ABSTRACT

This study characterizes the geochemistry and mineralogy of low-grade ore, muck-outs and tailings from a small-scale gold mining (SSGM) site in Paracale, Camarines Norte, and a large-scale gold mining (LSGM) operation in Aroroy, Masbate, to identify possible environmental hazards and resource-recovery potential. Samples were analyzed by inductively coupled plasma mass spectrometry (ICP-MS), direct mercury analysis, fire assay, X-ray diffraction (XRD), reflected-light petrography, automated scanning electron microscopy (Zeiss Mineralogic), and sieve-hydrometer grain-size analysis. The two sites differ in composition and mineralogy. Paracale tailings (n = 4) retain precious and base metals, with medians of 8.64 g/t Au (range: 12.56), 46.48 g/t Ag (range: 341.54), and 0.45% Cu (range: 1.14), in a siliceous matrix (71.30-79.92% SiO_2). Paracale tailings contain liberated electrum, refractory tellurides, and mercury-bearing Au-Ag amalgam particles, with accessory uraninite and monazite in the fine (< 63 µm) fraction examined. In contrast, Masbate tailings (n = 3) contain medians of 0.20 g/t Au (range: 0.08) and 0.74 g/t Ag (range: 0.12) in an aluminosilicate matrix with calcium oxide (2.58-4.52% CaO). Gold occurs within sulfides, mainly arsenian pyrite, and rare-earth-element phosphates are also present. Paracale tailings contain high concentrations of potentially toxic elements, including medians of 35.05 mg/kg total mercury (THg; range: 96.71), 5,000.00 mg/kg Pb (range: 4,751.90), and 1,876.45 mg/kg As (range: 6,609.40). Masbate shows localized arsenic enrichment, with medians of 128.60 mg/kg As (range: 44.20) in tailings and 483.80 mg/kg As (range: 903.20) in low-grade ore. These results provide a comparative baseline for the sampled materials; broader spatial sampling is needed for any regional assessment. Paracale tailings may be a candidate for secondary metal recovery and targeted remediation, whereas Masbate's arsenic-bearing wastes may require groundwater monitoring and containment. These contrasting profiles provide a basis for later evaluation of technologies such as green lixiviants for tailings management and resource recovery.

*Corresponding author
Email Address: **jhcgervasio@pnri.dost.gov.ph**
Date received: 31 May 2026
Dates revised: 04 August 2026; 16 September 2026
Date accepted: 12 October 2026
DOI: https://doi.org/10.54645/202619SupRQV-61

INTRODUCTION

The Philippines is among the top five most mineralized countries globally, with an estimated US$1 trillion of untapped metallic resources (Bunye 2018). The country currently has 60 operating metallic mines, 11 of them large-scale, as well as several thousand

KEYWORDS

Nuclear analytical techniques, environmental geochemistry, uraninite and Rare Earth Elements (REEs), mining tailings, Potentially Toxic Elements (PTEs), Small-Scale Gold Mining (SSGM)

small-scale mines that provide local livelihoods and national tax revenue (Johnson et al. 2025; National Economic Development Authority et al. 2022). World-class epithermal lode and placer gold deposits occur across the archipelago, mainly in five districts along or near the Philippine Fault: Baguio-Mankayan, Paracale, Masbate, Surigao, and Masara (Gabo-Ratio et al. 2020).

Despite these contributions, gold mining generates large volumes of tailings, the finely ground waste left after valuable metals are extracted from ore (Jenkin et al. 2024; Uy 2021). Tailings can pose serious risks to human health and ecosystems because they often contain potentially toxic elements (PTEs) and can generate acid mine drainage (Vriens et al. 2020). Tailings storage facilities (TSFs) also occupy large areas and can fail catastrophically, causing widespread contamination and heavy economic losses (Cacciuttolo et al. 2024). These concerns are greater in SSGM, where mercury amalgamation causes direct, unregulated emissions to air and water (Samaniego & Tanchuling 2018).

To mitigate these hazards, recent research has focused on reducing tailings volumes through reuse and on stabilizing TSFs structurally and geochemically. For example, mine tailings have been used as partial replacements for cement and sand in concrete (Ndikumana et al. 2024; Tan et al. 2025). Geotechnical monitoring and remote sensing, including unmanned aerial vehicles and artificial intelligence, are being used to monitor TSF integrity (Cacciuttolo et al. 2024), and geochemical remediation now includes bioremediation, phytostabilization, and chemical amendments to neutralize acidity (Putra et al. 2024). Leaching of PTEs with deep eutectic solvents (DES) is a promising route to both decontamination and resource recovery (Aglibot et al. 2025). However, any stabilization, remediation, or reprocessing approach depends on a thorough characterization of the waste, which is needed to select methods suited to its physicochemical and mineralogical properties.

Tailings characteristics vary with operational scale, location, and processing method. Large-scale gold mining (LSGM) is highly mechanized and uses multi-stage crushing, grinding and cyanidation circuits to maximize gold liberation under environmental controls (Khuduwe 2024). In contrast, SSGM relies on manual labor and simple tools and is governed by the People's Small-Scale Mining Act of 1991 (Republic Act 7076); it typically uses simple ball mills, sluicing, and open-air mercury amalgamation without emission controls (Clemente & Lanticse 2001). Although tailings reuse, monitoring, and stabilization have been studied widely, comparative data on the physicochemical and mineralogical properties of tailings and associated low-grade ores from SSGM and LSGM operations in the Philippines are limited. National statistics on mine waste exist, but detailed site-specific mineralogical and geochemical comparisons of artisanal and industrial systems are scarce. Without such data, containment designs and the evaluation of secondary-resource recovery, for example with green lixiviants, cannot account for differences in matrix behavior such as the siliceous SSGM wastes versus the carbonate-bearing LSGM wastes.

This study compares one SSGM site (Paracale) and one LSGM operation (Masbate), both in low-sulfidation epithermal gold districts but with different host rocks and extraction scales. The comparison describes how the two sites differ in composition and mineralogy, but it cannot separate the effects of operational scale from those of geology.

This study investigates the physicochemical and mineralogical characteristics of tailings from an SSGM site in Paracale, Camarines Norte, and an LSGM facility in Aroroy, Masbate, and of the associated low-grade ore and muck-outs, using analytical techniques. Specifically, it aimed to (1) characterize the geochemistry and mineralogy of the tailings, low-grade ore, and muck-outs; (2) compare materials from the SSGM and LSGM settings; and (3) identify potential environmental hazards and establish a baseline for evaluating future resource recovery and remediation, including with green lixiviants.

Geology and Ore Characteristics of Paracale and Masbate

The Paracale mining district is located within the Ancient Southeastern Luzon Arc, also referred to as the Quezon–Camarines Norte Block, and is tectonically bounded by the Philippine Trench to the east and the sinistral Philippine Fault Zone to the west (Casulla & Mizunaga 2023). The district is centered on the Paracale Trondhjemite, an Early to Middle Miocene granodioritic to trondhjemitic intrusion that forms a core antiform. It intrudes older basement rocks: the Cretaceous Cadig Ophiolite Complex (serpentinized harzburgite, peridotite, and gabbro) and the Jurassic Malaguit Schist (Casulla & Mizunaga 2023; Gibaga et al. 2026; Mitchell & Balce 1990; Mitchell & Carlile 1994). As a felsic intrusion, the Paracale Trondhjemite contains primary accessory minerals such as epidote, apatite, titanite, rutile, zircon, and opaque minerals (Giese et al. 1986; Mitchell & Balce 1990). This accessory mineralogy may be the source of the dense, refractory U- and REE-bearing minerals found in the waste. The basement is overlain by Cretaceous to Quaternary units, including the Cretaceous Tigninan Formation, the Eocene Tumbaga Formation (sedimentary clastics and limestone), the Miocene Bosigon Formation, the Tamisan Diorite, and the Pliocene to Quaternary Labo Volcanic Complex (andesites, dacites, and pyroclastic deposits) (Casulla & Mizunaga 2023; Gibaga et al. 2026).

Gold mineralization in the Paracale-Gumaus area is dominated by low-sulfidation epithermal Au-Ag veins (Gibaga et al. 2026; Mitchell & Balce 1990). Nearby systems include pyritic Au-Cu-Te veins at Exciban (James & Fuchs 1990) and Cu-Au-Fe magnetite-garnet skarns at Larap/Mabilo (Casulla & Mizunaga 2023). The mineralization is structurally controlled, along brittle faults, fissure-filling fractures, and lithological contacts, particularly at the margins of the Paracale Trondhjemite, the serpentinized harzburgites, and the siltstones and tuffs of the Tumbaga and Bosigon formations (Casulla & Mizunaga 2023; Gibaga et al. 2026; James & Fuchs 1990; Sillitoe 1991).

Paracale ores occur mainly as fissure-filling quartz veins, stockworks, and local breccias. The veins consist of massive white quartz, chalcedonic quartz, and drusy open-space fillings (Gibaga et al. 2026; Mines and Geosciences Bureau 2010). The principal ore minerals are native gold and electrum, occurring as disseminated free grains, drusy fillings in quartz, and inclusions in or between sulfide grains (Gibaga et al. 2026; James & Fuchs 1990). The sulfides are mainly coarse pyrite, with subordinate pyrrhotite, chalcopyrite, bornite, galena, sphalerite, arsenopyrite, covellite, and tetrahedrite (Gibaga et al. 2026). In the nearby, tellurium-bearing Exciban vein system, gold is closely associated with bismuth tellurides, including tellurobismuthite (Bi_2Te_3), hedleyite (Bi_7Te_3), and tetradymite (Bi_2Te_2S) (James & Fuchs 1990). Gangue minerals are mainly quartz, calcite, dolomite, and alteration clays such as illite and chlorite (Gibaga et al. 2026; James & Fuchs 1990; Mitchell & Balce 1990).

Because SSGM processing in Paracale is inefficient, the tailings retain high precious-metal grades, averaging 26.9 g/t Au and 65.6 g/t Ag (n = 4), together with base metals and PTEs, including up to 7,651 mg/kg Pb, up to 1,447 mg/kg As, about 0.24% Cu, and Zn and Hg (Gibaga et al. 2026). These characteristics make the tailings both an environmental concern and a possible secondary resource.

The Aroroy Mineral District, in northwestern Masbate Island, lies in an arc-basin terrane along the central segment of the Philippine Fault Zone. Deformation is transtensional, with dominant northwest-trending strike-slip structures and subordinate northeast-striking faults. The basement consists of pre-Cenozoic schists (Bale Schist) and metabasic rocks to gabbro (Manapao Basalt), intruded by the Eocene Aroroy Quartz Diorite, a hornblende quartz diorite. It is unconformably overlain by an Eocene to Pliocene volcano-sedimentary succession: the Kaal Formation (shale, sandstone, conglomerate, and andesitic to basaltic flows), the Middle Miocene Lanang Formation (volcanic conglomerate, tuffaceous sandstone, shale, and calc-arenite), and the Early Pliocene Nabongsuran Andesite (augite-hornblende porphyritic flows, plugs, and pyroclastic rocks) (Carranza 2010; Garagan et al. 2016; Johnson et al. 2025).

The Masbate Gold Project is a low-sulfidation epithermal Au-Ag deposit system (Carranza 2010; Garagan et al. 2016; Johnson et al. 2025). Mineralization is controlled by major structures (Main Vein, Colorado, Montana, Pajo, and Blue Quartz), which host quartz vein arrays, stockworks, sheeted veinlets, and breccia zones up to about 2 km long and 20-75 m wide (Garagan et al. 2016; Johnson et al. 2025). The main host rocks are monomictic to polymictic andesitic volcaniclastics and coherent andesite flows, domes, and plugs of the Nabongsuran Andesite and Lanang Formation, and locally the Aroroy Quartz Diorite. Barren augite-hornblende porphyry plugs and dikes cut the mineralized structures and record syn- to post-mineralization intrusion (Johnson et al. 2025).

Masbate ores contain mainly fine-grained electrum, an Au-Ag alloy with a fineness of about 500-600 (50-60 wt% Au; 40-50 wt% Ag) (Filminera Resources Corp. 2018; Garagan et al. 2016). Electrum commonly occurs as very fine inclusions (<10 µm) within pyrite or goethite, or along sulfide grain margins (Garagan et al. 2016). Sulfides make up generally 1-3% or less of the rock and are dominated by pyrite, with minor marcasite, chalcopyrite, galena, and sphalerite; goethite occurs in oxidized zones. Gangue minerals include grey chalcedonic, amorphous, banded, and cockscomb quartz, secondary K-feldspar or adularia, calcite, and chlorite. Alteration is zoned from silicic to argillic, with illite-smectite, chlorite, and sericite, and a prominent smectite-gypsum overprint (Garagan et al. 2016; Johnson et al. 2025). Average run-of-mine (ROM) ore grades are about 0.57-0.94 g/t Au (Filminera Resources Corp. 2018; Gibaga et al. 2026).

Extraction and Processing

Gold in Paracale is extracted by SSGM, which relies on whole-ore milling followed by mercury amalgamation (Gibaga et al. 2023, 2026; Samaniego & Tanchuling 2018). ROM ore is usually charged into small cylindrical ball mills with water and lime; the lime neutralizes acid produced by sulfide oxidation (Samaniego & Tanchuling 2018).

Liquid elemental mercury (Hg^0) is then added directly to the mill or pan, where it binds liberated gold to form an amalgam. The amalgam is recovered by panning and heated with a gasoline-air torch, usually with borax, to volatilize the mercury and produce a gold button. This step releases much of the mercury to the atmosphere; one estimate is that about 83% of the mercury used is emitted as Hg^0 vapor (Clemente & Lanticse 2001; Gibaga et al. 2023; Samaniego & Tanchuling 2018). In some Paracale operations, mercury-treated tailings are subsequently reprocessed by vat or carbon-in-pulp cyanidation to extract part of the residual gold left behind by amalgamation (represented by PAR-02 in this study). Because this secondary leaching is applied to the same ball-milled amalgamation residues and remains incomplete for enclosed or refractory grains, both amalgamation and cyanidation-reprocessed residues are discharged into the local SSGM ponds and are evaluated together here to capture the range of Paracale SSGM wastes.

This inefficiency strongly influences the composition and environmental behavior of the tailings. Amalgamation recovers coarse, liberated gold preferentially and performs poorly on fine gold or gold enclosed in sulfides, so overall recovery is low, about 27% (Gibaga et al. 2026). Consequently, much of the gold, together with silver and base-metal sulfides, stays in the tailings, which are commonly discharged into unlined, improvised containment such as earthen ponds, concrete boxes, or open grassland, without engineering controls (Gibaga et al. 2026; Samaniego & Tanchuling 2018). Wastewater and fine slurry may overflow into nearby streams (Luklukan Creek, the Gumaus River, and the Danao River) and finally reach Mambulao Bay (Gibaga et al. 2023). Reported values for the Paracale wastes include about 3,597 mg/L total suspended solids (TSS), 0.01-0.18 mg/L mercury in wastewater, 3.0-11.7 mg/kg mercury in sediments and solids, and substantial Pb, As, Cu, and Zn loads and fine sulfide particles (Gibaga et al. 2023, 2026; Samaniego & Tanchuling 2018).

In contrast, the Masbate LSGM operation uses mechanized open-pit hard-rock mining and an industrial carbon-in-leach (CIL) cyanidation circuit (Filminera Resources Corp. 2018; Garagan et al. 2016). The flowsheet comprises primary and secondary crushing, semi-autogenous grinding (SAG), wet ball-mill grinding to a target P80 of 106 µm (80% of the product passing 106 µm), and whole-ore cyanide leaching (Filminera Resources Corp. 2018; Johnson et al. 2025). The slurry is leached with sodium cyanide (NaCN) in CIL tanks for about 24 h, with lime added to maintain alkalinity and suppress hydrogen cyanide formation. Dissolved Au and Ag adsorb onto activated carbon, are stripped by elution, recovered by electrowinning, and smelted into gold-silver bullion (Filminera Resources Corp. 2018; Johnson et al. 2025). Before they are discharged to the tailings system, the leach residues are treated to detoxify residual cyanide (Johnson et al. 2025).

The Masbate circuit achieves much higher recoveries than the Paracale SSGM process: reported Au recoveries are about 65-89%, depending on oxidation state and ore domain (Garagan et al. 2016; Johnson et al. 2025). The tailings are pumped to an engineered tailings storage facility (TSF) of about 217 ha, with a dam about 44.3 m high, receiving roughly 7.3 million dry tonnes of solids per year (Filminera Resources Corp. 2018). In the TSF, solids settle and the decant water is recycled to the plant or treated before permitted discharge (Filminera Resources Corp. 2018). Waste rock is classified as potentially acid-generating (PAG) or non-acid-generating (NAG) from total sulfur (S_{TOT}) and total carbon (C_{TOT}), and PAG material is encapsulated in NAG rock in the waste dumps to limit acid rock drainage (ARD) (Garagan et al. 2016; Johnson et al. 2025). The efficient CIL recovery explains the low residual Au in the Masbate tailings (reported as 0.29-0.42 g/t; this study, median 0.20 g/t, range: 0.08) (Garagan et al. 2016; Johnson et al. 2025).

MATERIALS AND METHODS

Study Site

Tailings, low-grade ore, and muck-out samples were collected from an SSGM site in Paracale, Camarines Norte, in July 2024 (wet season), and from an LSGM site in Aroroy, Masbate, in May 2025 (transition from dry to wet season). These samples were newly collected for this study and are completely distinct from the sample sets analyzed in earlier studies of the district (Aglibot et al. 2025; Gibaga et al. 2023, 2026). The sampling locations are shown in **Figure 1**.

At the SSGM site, four tailings samples and two muck-out samples were collected (

Table 1). The tailings were obtained from two adjacent ponds with approximate surface areas of 500 m² and 300 m² and reported depths of 2–3 m. Two tailings samples were collected from each pond. The muck-outs were sampled from stockpiles near the underground tunnels. Muck-out is the waste material removed from an underground mine during excavation and may consist of broken rock, soil, clay, or low-grade mineralized material.

At the LSGM site, three tailings and two low-grade ore samples were collected (**Table 1**). The tailings were sampled along the perimeter of the tailings storage facility (TSF), which has an area of about 217 ha and a crest elevation of 67 mRL (Filminera Resources Corp. 2018; Johnson et al. 2025). The low-grade ore samples (MGP-04 and MGP-05) were collected from open-pit stockpiles designated as low-grade ore by the guiding mine personnel. Because the facilities are large, particularly the Masbate TSF, the sampling was limited to a few points and gives a preliminary characterization rather than a spatial profile of the waste.

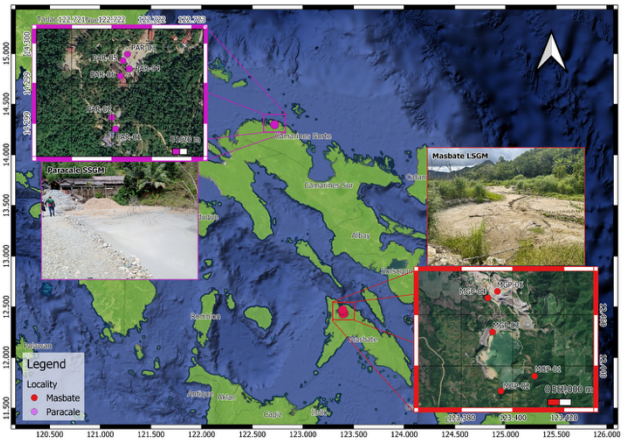


Figure 1: Location of the sampling sites at the Paracale SSGM (Camarines Norte) and Masbate LSGM (Aroroy, Masbate) operations.

Table 1: Summary of samples collected in Paracale and Masbate

Sample Name	Coordinates	Date Collected	Sample Description
Locality: SSGM in Paracale, Camarines Norte			
PAR-01	14° 17' 54.35" N, 122° 43' 17.57" E	17 July 2024	Tailings after mercury amalgamation
PAR-02	14°17' 54.86" N, 122° 43' 17.40" E	17 July 2024	Tailings that were reprocessed with cyanide after mercury amalgamation
PAR-03	14° 17' 57.70" N, 122° 43' 18.11" E	17 July 2024	Tailings after mercury amalgamation
PAR-04	14° 17' 57.05" N, 122° 43' 18.19" E	18 July 2024	Muck-outs
PAR-05	14° 17' 57.42" N, 122° 43' 17.91" E	18 July 2024	Tailings after mercury amalgamation
PAR-06	14° 17' 56.73" N, 122° 43' 17.79" E	18 July 2024	Muck-outs
Locality: LSGM in Aroroy, Masbate			
MGP-01	12° 26' 09.81" N, 123° 24' 30.71" E	28 May 2025	Tailings collected at the perimeter of ongoing tailings pond
MGP-02	12° 25' 48.94" N, 123° 23' 43.51" E	28 May 2025	Recent tailings (i.e., deposited in the year of sampling); relatively wet
MGP-03	12° 27' 11.74" N, 123° 23' 31.46" E	28 May 2025	Recent tailings; relatively dry
MGP-04	12° 27' 59.45" N, 123° 23' 24.98" E	28 May 2025	Low-grade ore stockpile
MGP-05	12° 28' 08.79" N, 123° 23' 38.57" E	28 May 2025	Low-grade ore; collected from the stockpile of recently blasted materials

Sample Collection

Tailings were sampled from the upper 20 cm of the ponds at both sites, and ore and muck-out samples were taken from stockpiles. Sacked tailings were also collected at the SSGM site (PAR-05). Samples were collected with a plastic trowel, placed in double-layered resealable polyethylene (PE) bags, and stored in rice sacks. Separate plastic trowels were used at each site, and they were washed with tap water and dried with paper towels between samples. Only a few samples could be collected because access to the mining zones was restricted. Given the small number of samples, the values should be treated as preliminary estimates and not as site-wide values.

At Paracale, six distinct sample IDs were collected. Each ID represented a separate 30 kg bulk sample assembled from multiple bags containing 10–12 kg of material to account for spatial variability. The same sampling approach was used at Masbate to collect five distinct samples, although each bulk sample weighed approximately 25 kg. All samples were subsequently homogenized and subsampled by coning and quartering.

Sample Preparation

Samples were prepared at the Philippine Nuclear Research Institute of the Department of Science and Technology (DOST-PNRI). Subsamples of the required mass were obtained by coning and quartering and air-dried at approximately 30°C for 10 days until a constant weight was reached.

At least 500 g of each tailings sample was sieved with a CISA BA 200N digital electromagnetic sieve shaker, using sieves of 4, 2, 1, 0.5, 0.25, 0.125, and 0.063 mm aperture, which separate the Wentworth (1922) size classes: pebbles (> 4 mm), granules (2-4 mm), very coarse sand (1-2 mm), coarse sand (0.5-1 mm), medium

sand (0.25-0.5 mm), fine sand (0.125-0.25 mm), very fine sand (0.063-0.125 mm), and mud (< 0.063 mm).

A second 500 g portion of each air-dried tailings sample, and the rock samples, were pulverized for 10 min in a RockLabs benchtop ring mill and used for geochemical analysis by ICP-MS, direct mercury analysis (DMA), and fire assay with atomic absorption spectrometry (FA-AAS). The ring mill was made of chrome steel, an alloy containing Fe, Cr, and C. To minimize cross-contamination, quartz-rich sand was pulverized between samples to scour the mill. The mill was then washed with soap and tap water and wiped with ethanol.

The < 63 µm fraction of the sieved tailings was used for X-ray diffraction (XRD) to improve powder averaging, reduce microabsorption and the preferred orientation of platy minerals, and thereby improve phase identification (Ali et al. 2022; Kleeberg et al. 2008). Using the sieved fraction rather than pulverized material also avoids the strain, peak broadening, and local amorphization caused by intensive milling (Baláž 2008). The pulverized rock samples were analyzed by XRD as well.

The < 63 µm fraction of each sample was mounted in epoxy and polished following Craig & Vaughan (1994) and Goodall et al. (2005). Approximately 2.0 g of sample was used to prepare each disk, which measured 2 cm in diameter and 1 cm in height. Buehler EpoxiCure 2 hardener and resin were mixed at a 1:4 ratio. Each sample was thoroughly combined with the epoxy mixture, poured into a silicone mold, and cured for 24 h in a vacuum chamber at approximately -12 psi and 30°C. The cured disks were then diamond-polished to a final grit size of 1 µm using an EcoMet 30 grinder-polisher. For the Masbate low-grade ore sample MGP-05, an additional mineral-concentrate disk was prepared to facilitate the identification of sparse gold-bearing phases: subsamples chipped with a geological hammer were pulverized in the ring mill and manually panned with water to collect the dense mineral fraction, after which a hand magnet was used to remove magnetic grains and isolate the non-magnetic heavy fraction prior to epoxy mounting and polishing.

In addition, thin sections were prepared from fist-sized or larger pieces of the low-grade ores. Zones with visible sulfides or metallic grains were cut into slabs of about 3 × 1 × 0.5 cm, mounted on glass slides, and polished to a thickness of about 30 µm. The thin sections and epoxy disks were first examined with a petrographic microscope and then coated with about 30 nm of carbon before automated mineralogical analysis (Zeiss Mineralogic).

Mineralogical Analysis

The < 63 µm fraction of the tailings and the pulverized rock samples were analyzed by XRD with a Shimadzu MAXima_X XRD-7000 at the National Institute of Geological Sciences, University of the Philippines Diliman (UPD-NIGS), using a Cu anode (Cu $K\alpha_1$ radiation, $\lambda = 1.5406$ Å). Each sample was scanned continuously from 3° to 90° 2θ at 2° min^{-1}, at 30 kV and 20 mA. The instrument was checked with a silicon powder standard: measured 2θ angles and d-spacings were compared with the reference values and found to be within the acceptable range (±0.05 tolerance on 14 October 2025). Phases were identified by searching the three strongest d-spacings (Hanawalt method) in the WebMineral and RRUFF databases, with QualX, and the diffractograms were interpreted with Match! version 4 (Crystal Impact).

Polished thin sections and disks were examined at DOST-PNRI with Nikon Eclipse LV100N POL LED and Ci-POL polarizing microscopes, in transmitted and reflected light at up to 1,000× magnification. Minerals and textures were identified with reference to Castroviejo (2023), Ineson (1989), Kerr (1977), Nesse (2020), Pracejus (2015), and Spry & Gedlinske (1987).

Polished thin sections and disks were imaged and analyzed on a ZEISS Sigma 300 VP scanning electron microscope (SEM) (University of Leicester, UK) with two Bruker XFlash 6-60 energy-dispersive X-ray (EDS) detectors. The samples were first scanned with Zeiss Mineralogic V01.06 automated mineralogy software, using a grey-scale filter on the backscattered-electron (BSE) image so that only bright, high-atomic-number phases were analyzed. The scan used a 20 kV accelerating voltage, a 120 µm aperture, an 8.5 mm working distance, a dwell time of 0.07 s per pixel, and a 5 µm step size. Minerals were classified with the standard Zeiss Mineralogic "Mining" recipe, which defines elemental ranges for minerals common in ore deposits. For each sample, single-point EDS analyses of the bright phases found in the scan were done at the same accelerating voltage but with a 30 µm aperture. The number of analyzed points varied considerably among samples, as some samples were successfully scanned in their entirety using automated mineralogy, whereas others were only partially scanned. The selected mineral phases primarily included those associated with gold occurrences, along with other phases considered noteworthy based on their apparent rarity or potentially significant characteristics.

The EDS spectra were processed and quantified in Bruker ESPRIT 3.3 with a ZAF correction, and element concentrations are reported in weight percent. The samples were carbon-coated to 30 nm (Agar Auto Carbon Coater), mounted on a 5 × 5 cm stage, and fixed with carbon tape to improve conductivity (Eberle et al. 2017).

Grain Size Analysis

Grain-size analysis was done at DOST-PNRI by sieving and hydrometer methods according to ASTM D6913 and D7928 (ASTM International). The dried tailings were sieved for 10 min at the maximum vibration amplitude of 2 mm. The mass of each sieve was recorded before and after sieving, and the percent passing each sieve was calculated as:

$$P_i = \left(1 - \frac{\sum_{k=1}^{i} W_k}{W_T}\right) \times 100$$

(Equation 1)

where: P_i is the percentage passing sieve i, W_T is the total mass of the sample, W_k is the mass retained on sieve k, and $\sum_{k=1}^{i} W_k$ is the cumulative mass retained from the top sieve down to sieve i (Hossain et al. 2021b).

Samples with at least 50 g of material in the pan (< 63 µm) after sieving (PAR-05 and MGP-03) were subjected to hydrometer analysis with an ASTM 152H hydrometer, using 125 mL 4% sodium hexametaphosphate (Calgon) solution as the dispersing agent. Hydrometer readings were taken at 1, 2, 4, 8, 15, 30, 60, 120, 240 and 1,440 min, and the temperature was recorded for the density and viscosity corrections. The percent finer was calculated as:

$$P = \left(\frac{100}{W_s}\right) a R_c$$

(Equation 2)

where: P is the percent finer, a is the correction factor, R_c is the corrected hydrometer reading, and W_s is the mass of the dried tailings (Deiss 2025; Hossain et al. 2021a). The data are shown as a grain-size distribution curve and on a USDA sand-silt-clay texture triangle (Bhandari & Dhakal 2021).

The coefficients of uniformity (Cu) and curvature (Cc) indicate whether the material is well graded or poorly graded. They use D60, D30 and D10, the particle diameters for which 60%, 30% and

10% of the sample (by mass) is finer. The C_u and Cc are computed based on the following equations:

$$C_u = \frac{D_{60}}{D_{10}} \quad \textbf{(Equation 3)}$$

$$C_c = \frac{(D_{30})^2}{D_{60} \times D_{10}} \quad \textbf{(Equation 4)}$$

Table S1 gives the criteria for interpreting C_u and C_c.

Geochemical Analysis

Elemental concentrations were determined by four-acid digestion (using hydrochloric, nitric, perchloric, and hydrofluoric acids) followed by inductively coupled plasma mass spectrometry (ICP-MS) at Intertek Testing Services Philippines, Inc., to which at least 20 g of each pulverized sample was sent. A blank was run before analysis, and the certified reference materials (CRMs) OREAS 44P, 601d, 603b, 624 and 90 were analyzed at the start of the batch for quality control; recoveries are given in **Table S2**.

Total mercury (THg) was measured with a direct mercury analyzer (DMA; Milestone DMA-80 evo) following US EPA Method 7473, which determines Hg in solids and solutions by thermal decomposition (up to 900 °C), amalgamation, and atomic absorption spectrophotometry. The pulverized Paracale samples were diluted to 10% (w/w) with silica (SiO_2, 99.7%) powder, and at least 0.1 g of the dilution was weighed into a nickel boat and loaded into the autosampler (Samaniego et al., 2020). The Masbate samples were not diluted because they had low THg concentrations. Each batch started with a blank, followed by the stream-sediment CRM GSD-1 (102% recovery).

Gold was determined by fire assay of a 50 g portion of each sample at Intertek Testing Services Philippines, Inc. A blank run before the samples gave a result below the detection limit (< 0.005 mg/kg Au). The results were checked with CRM OREAS 250 following the method of Gibaga et al. (2023). The CRM has a certified value of 0.309 mg/kg Au; the measured value was 0.328 mg/kg (106% recovery).

Pollution Assessment

The enrichment factor (EF) and the geoaccumulation index (Igeo) were calculated for potentially toxic elements (PTEs) in the SSGM and LSGM samples. EF compares the concentration of an element, normalized to a conservative reference element, with its background value, and is used to indicate enrichment relative to the background. A reference element, usually Sc, Al, or Ti, is chosen for its geochemical stability and predominantly crustal origin. In this study, Sc was used as a normalizer element because it is highly inert, resistant to weathering, and structurally stable across varying sediment grain sizes (Aglibot et al. 2025; Bautista et al. 2024; dela Cruz et al. 2025; Gibaga et al. 2022; Reimann & Caritat 2000; Zhao et al. 2023). The EF formula is shown in **Equation 5**.

$$\text{EF} = \frac{(x_i/RE)_{sample}}{(x_i/RE)_{background}} \quad \textbf{(Equation 5)}$$

where: x_i and RE are the concentrations of the element of interest and of the reference element, in the sample and in the background (Buat-Menard & Chesselet 1979). The EF values were assigned to the five enrichment categories of Sutherland (2000) (**Table 2**).

The geoaccumulation index compares the measured concentration of an element (C_n) with its background concentration (B_n):

$$I_{geo} = \log_2 \frac{C_n}{1.5B_n}$$

(Equation 6; Müller 1969**),**

where the factor 1.5 allows for natural variation of the background. Background concentrations for both indices were taken from the average upper continental crust (UCC) of Rudnick & Gao (2014), because no local or national geochemical baseline exists for this kind of material. Because the analyzed samples are mineralized ores, muck-outs, and tailings rather than receiving soils or sediments, EF and I_{geo} values reported here reflect geochemical enrichment of the waste materials relative to the average upper continental crust rather than environmental pollution of a surrounding ecosystem. The seven I_{geo} classes of Müller (1969) are listed in the first two columns of **Table 3**.

Table 2: EF values of PTEs from the Paracale SSGM and Masbate LSGM. The class of a group is based on the median EF.

EF Value	Description	Paracale SSGM		Masbate LSGM	
		Tailings (n=4)	Muck-outs (n=2)	Tailings (n=3)	Low-grade ore (n=2)
EF < 2	Deficiently to minimal enrichment			Ni, Co, Cr, Zn	Ni, Co, Cr, Pb, Zn
2 ≤ EF < 5	Moderate enrichment	Co	Co	Cu, Cd	Cu, Cd
5 ≤ EF < 20	Significant enrichment	Ni, Cr	Ni	Hg, Pb, Sb	Hg
20 ≤ EF < 40	Very high enrichment		Cr	As	
EF ≥ 40	Extremely high enrichment	Hg, Cu, Pb, As, Cd, Sb, Zn	Hg, Cu, Pb, As, Cd, Sb, Zn		As, Sb

Table 3: I_{geo} values of PTEs from the Paracale SSGM and Masbate LSGM

I_{geo} Value	I_{geo} Class	Description	Paracale SSGM		Masbate LSGM	
			Tailings (n=4)	Muck-outs (n=2)	Tailings (n=3)	Low-grade ore (n=2)
$I_{geo} \leq 0$	0	Uncontaminated	Cr, Co	Ni, Co	Cr, Ni, Co	Pb, Cr, Zn, Ni, Co
$0 < I_{geo} \leq 1$	1	Uncontaminated to moderately contaminated	Ni	Cr	Zn	Cu
$1 < I_{geo} \leq 2$	2	Moderately contaminated			Cu, Cd	Cd
$2 < I_{geo} \leq 3$	3	Moderately to strongly contaminated			Pb	Hg

$3 < I_{geo} \leq 4$	4	Strongly contaminated		Hg	Hg, Sb	
$4 < I_{geo} \leq 5$	5	Strongly to extremely contaminated			As	
$I_{geo} > 5$	6	Extremely contaminated	Hg, Cu, Pb, As, Cd, Sb, Zn	Cu, Pb, As, Cd, Sb, Zn		As, Sb

RESULTS AND DISCUSSION

Mineralogical Composition

The mineralogy of the Paracale and Masbate materials was determined by petrographic microscopy, XRD, and scanning electron microscopy (SEM). Reflected-light microscopy was used mainly to locate grains that might contain Au for SEM analysis of their mode of occurrence (liberated or enclosed in another mineral). Together, the results describe the main ore minerals and post-mining alteration in the wastes, which influence their behavior during processing and weathering.

Table 4 summarizes the petrographic observations. Pyrite and chalcopyrite are the main sulfides at both sites; bornite, magnetite, and hematite are minor. In Paracale, this assemblage is consistent with the epithermal, tellurium-bearing veins of the district (Gibaga et al. 2026; Mitchell & Balce 1990). In Masbate, it is consistent with the low-sulfidation epithermal deposit of the Aroroy district (Carranza 2010; Garagan et al. 2016; Johnson et al. 2025).

Table 4: Summary of petrographic observations.

Sample ID	Type	Format	Primary Minerals	Accessory/Minor/ Secondary Minerals	Key Textures and Notes
Paracale SSGM					
PAR-06	Muck-out	Disk	Pyrite, magnetite	-	Inhomogeneous grain size (unsieved).
PAR-01, 02, 03, 05	Tailings	Disk	Pyrite, chalcopyrite	Magnetite, bornite, hematite	"Gnawed" and tarnished hematites observed.
Masbate LSGM					
MGP-04, 05	Low-grade ore	Disk and thin section (Note: The disk of MGP-05 is composed of concentrated low-grade ore)	Pyrite, chalcopyrite	Hematite	Mosaic texture in veinlets; exsolution lamellae; dogtooth texture.
MGP-01, 02, 03	Tailings	Disk	Pyrite	Magnetite, chalcopyrite, bornite, hematite	Martitization; "gnawed" and porous/pitted hematite; euhedral pyrite; orange-brown tarnished pyrite in plane-polarized reflected light.

At Paracale, the XRD patterns (**Figure 2**) show gangue dominated by quartz and plagioclase, with biotite or muscovite as the mica phase (**Table 5**). Gold in the Paracale tailings occurs in both liberated and enclosed forms. This applies to the <63 µm fraction only. Some of the gold occurs as free-milling electrum grains, with compositions from $Au_{5.36}Ag$ to Au_2Ag and $Au_{1.36}Ag$. Other electrum grains are enclosed in quartz (**Figure 3)** or in complex Mn-Zn-Co-Ni oxides.

The Hg-bearing Au–Ag particles ($AgAu_5Hg_2$) indicate two distinct sources of recovery loss. First, some gold remained enclosed in gangue and was therefore unavailable for amalgamation, demonstrating incomplete liberation during whole-ore milling. Second, amalgam particles present in the tailings show that some liberated gold reacted with mercury but was not recovered during subsequent separation.

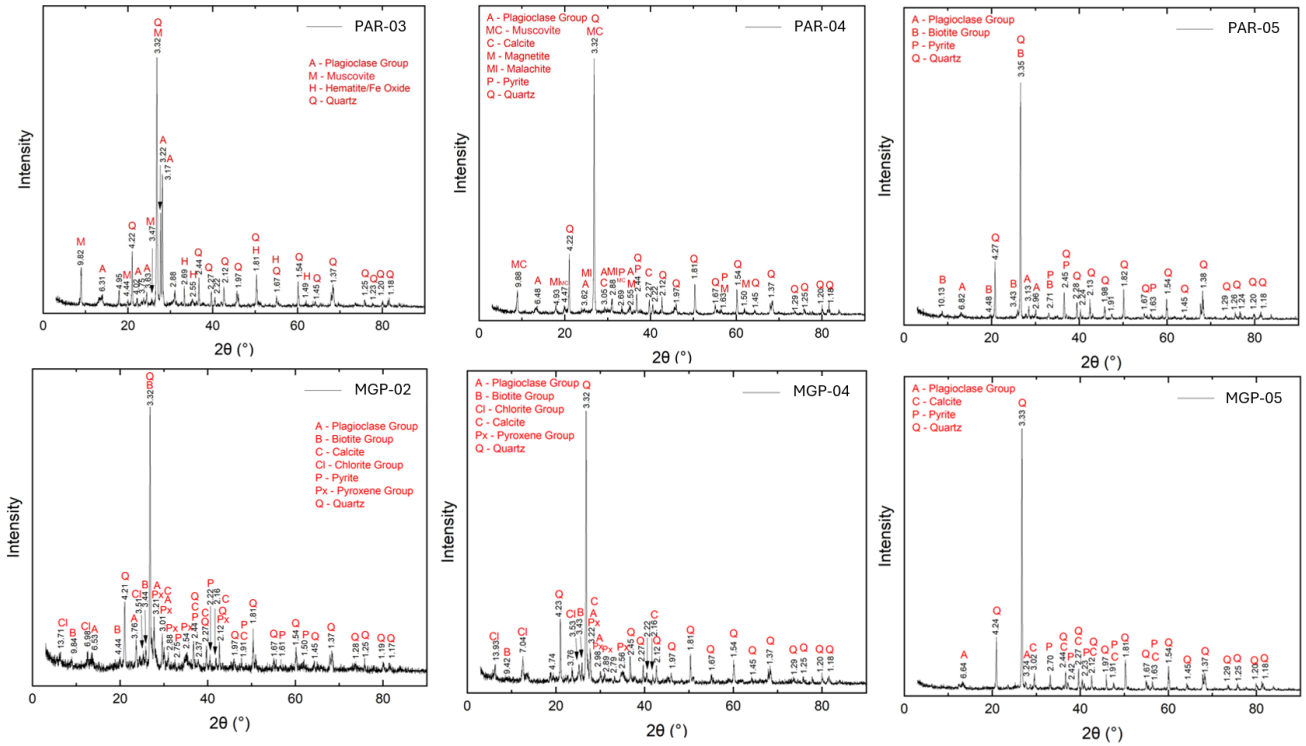


Figure 2: XRD patterns of representative tailings and muck-out or low-grade ore samples from the Paracale SSGM and Masbate LSGM sites.

Table 5. Summary of mineral phases identified by qualitative XRD analysis. Phases present at concentrations below approximately 1–2% may not be detected.

Sample ID	Sample Type	Dominant Silicates	Mica Phase	Accessory/Minor/Other Phases
Paracale SSGM				
PAR-01	Tailings	Quartz, plagioclase	Biotite	Pyrite
PAR-02	Tailings	Quartz, plagioclase	Biotite	None identified
PAR-03	Tailings	Quartz, plagioclase	Muscovite	Hematite/Fe oxide
PAR-04	Muck-out	Quartz, plagioclase	Muscovite	Calcite, magnetite, malachite, pyrite
PAR-05	Tailings	Quartz, plagioclase	Biotite	Pyrite
PAR-06	Muck-out	Quartz	Muscovite	None identified
Masbate LSGM				
MGP-01	Tailings	Quartz, plagioclase	None	Calcite
MGP-02	Tailings	Quartz, plagioclase	Biotite	Calcite, chlorite, pyrite, pyroxene
MGP-03	Tailings	Quartz, plagioclase	Biotite	Calcite, chlorite, pyrite
MGP-04	Low-grade ore	Quartz, plagioclase	Biotite	Calcite, chlorite, pyroxene
MGP-05	Low-grade ore	Quartz, plagioclase	None	Calcite, pyrite

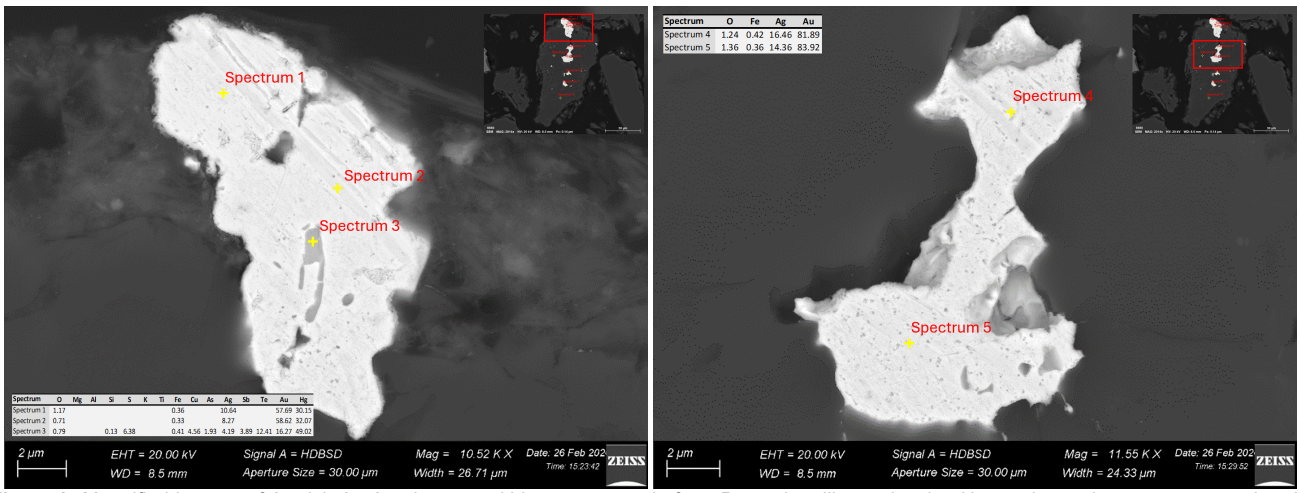


Figure 3: Magnified images of Au-rich Au-Ag electrum within a quartz grain from Paracale tailings, showing Hg amalgamation on an exposed grain (left) and an unmodified enclosed grain (right). Both images are from PAR-01 disk.

The Paracale samples also contain gold-silver tellurides: sylvanite and petzite (Au-Ag tellurides) and the Ag telluride hessite (**Figure 4)**. Tellurides are refractory to amalgamation and are slow to leach by cyanide (Yang et al. 2021; Zhang et al. 2010), so they may contribute to the high residual gold and silver grades of the tailings. One grain is a Hg-rich Au-Ag telluride, which may indicate reaction of a primary telluride with mercury during milling. These mineralogical observations are supported by bulk ICP-MS data (**Table S5**), which reveal substantial tellurium enrichment in the Paracale wastes (median 9.71 mg/kg Te, range: 92.15 in tailings; median 40.21 mg/kg Te, range: 78.66 in muck-outs) compared to the Masbate wastes (median 0.73 mg/kg Te in tailings; 0.58 mg/kg in low-grade ore), consistent with the refractory telluride phases documented in the Paracale district. The uraninite, enriched in Y and Dy (**Figure S1**), and the Ce-dominant monazite (**Figure S2**) in the Paracale tailings are not expected from low-sulfidation epithermal fluids, which typically do not transport significant U or rare earth elements (REE) (Louvel et al. 2022; Seward et al. 2014). They are interpreted as inherited accessory minerals from the host rock, the Paracale Trondhjemite, a felsic intrusion (Sajona & Maury 1998) that contains accessory apatite, zircon, titanite, and opaque minerals (Giese et al. 1986). Because the veins fill faults and contacts at the margin of the intrusion (Casulla & Mizunaga 2023; Gibaga et al. 2026), some trondhjemite wall rock and fault gouge are extracted with the ore. Milling liberates the dense, refractory accessory minerals from this rock, and they pass into the tailings. These phases are mineralogical occurrences only. Because they were detected as discrete grains in the SEM scan without any quantification of their abundance or distribution, their economic significance or radiological relevance cannot be assessed. Bulk ICP-MS analyses (**Table S5**) confirm quantifiable concentrations of uranium and thorium in the Paracale tailings (median 1.11 mg/kg U, range: 7.09; median 0.96 mg/kg Th, range: 0.57) and muck-outs (median 0.21 mg/kg U, range: 0.16; median 0.37 mg/kg Th, range: 0.28), as well as in the Masbate tailings (median 0.66 mg/kg U, range: 0.04; median 1.39 mg/kg Th, range: 0.41) and low-grade ore (median 0.45 mg/kg U, range: 0.48; median 0.74 mg/kg Th, range: 0.85). The elevated maximum U in the Paracale tailings (up to 7.30 mg/kg; mean 2.54 mg/kg) aligns with the SEM identification of discrete uraninite grains (~80 wt% U; **Figure S1)** which may have originated from the trondhjemite wall rock, while confirming that the bulk wastes remain within the typical upper continental crust levels (UCC: 2.7 mg/kg U, 10.5 mg/kg Th; Rudnick & Gao 2014) and do not pose bulk radiological hazards.

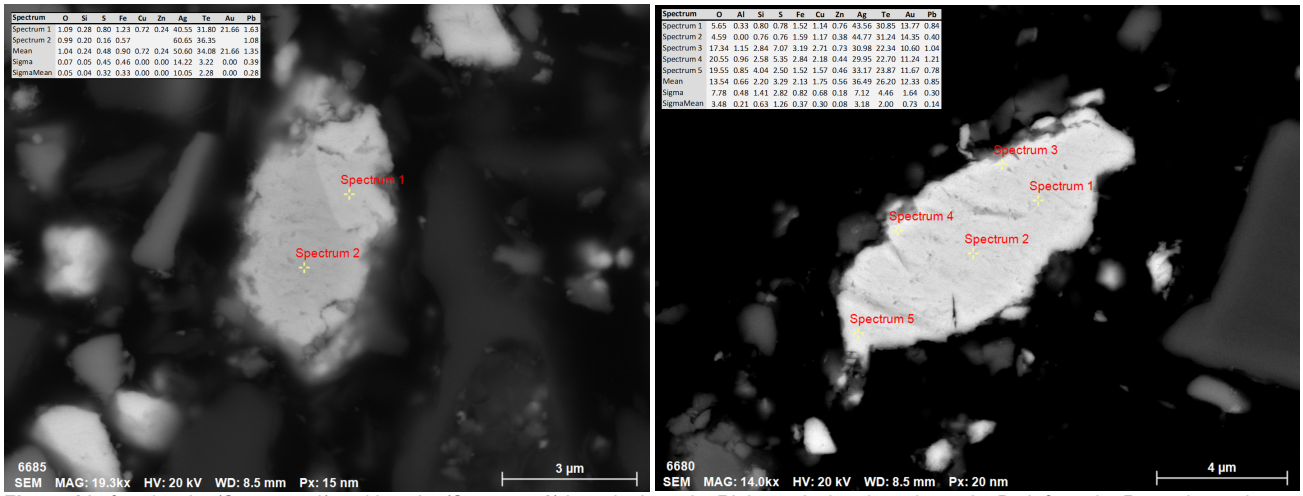


Figure 4 Left: sylvanite (Spectrum 1) and hessite (Spectrum 2) in a single grain. Right: an isolated petzite grain. Both from the Paracale muck-outs (PAR-06 disk).

The Masbate samples differ in several respects. The XRD patterns (**Figure 2**) show quartz and plagioclase, with biotite as the only mica, accompanied by calcite, chlorite, and pyroxene (**Table 5**). No liberated native gold was found in the scan of the Masbate tailings. Gold-rich electrum was found only in the concentrated low-grade ore, in arsenian pyrite (about 1% As) and in pyrite (**Figure 5)**. This suggests that gold in the Masbate ore is not free-milling and that its recovery depends on grinding fine enough to expose the gold in the sulfides, consistent with the fine grind (P80 = 106 µm) used by the operation (Filminera Resources Corp. 2018; Garagan et al. 2016). Primary microtextures observed in the low-grade ore include exsolution lamellae between Cu-Fe sulfides (chalcopyrite and bornite), mosaic textures in veinlets, and dogtooth texture. These textures provide insights into the ore-forming conditions and post- depositional processes including mineral cooling, recrystallization, and the redistribution of copper and iron within sulfide phases. In addition, automated SEM-EDS analysis of the Masbate low-grade ore thin section (MGP-05) identified trace rare earth element (REE) phosphate grains, including Ce-dominant monazite adjacent to pyrrhotite and an REE-Ti phosphate phase (**Figure S3**), which are supported by bulk ICP-MS concentrations across the Masbate materials (**Table S5**; median 18.86 mg/kg Ce, 2.42 mg/kg Dy, 9.28 mg/kg La, 10.48 mg/kg Nd, and 11.97 mg/kg Y in tailings).

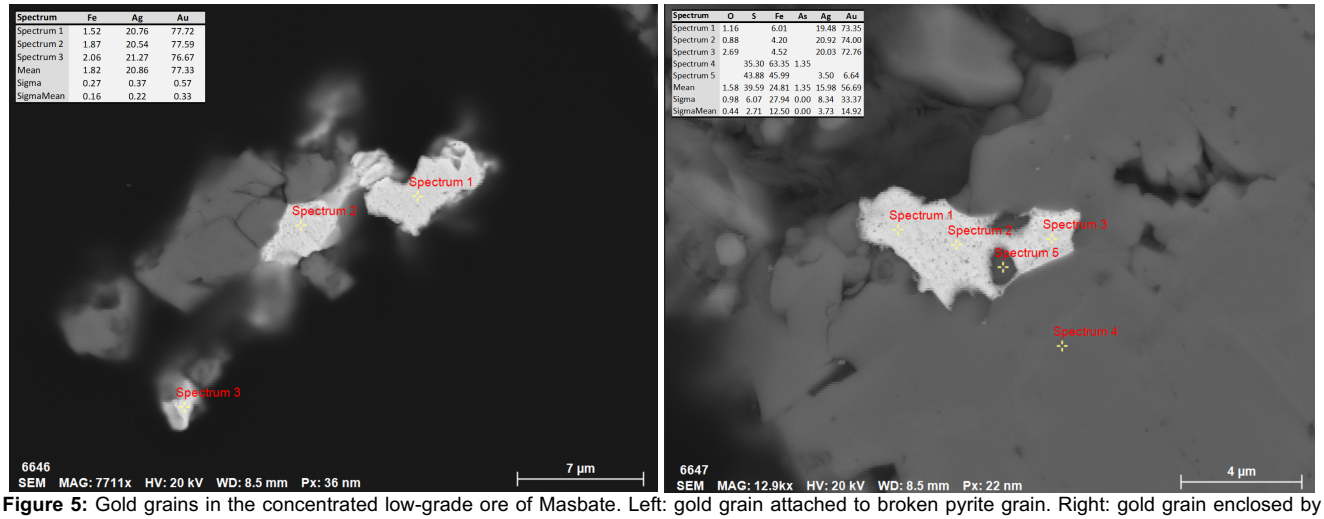


Figure 5: Gold grains in the concentrated low-grade ore of Masbate. Left: gold grain attached to broken pyrite grain. Right: gold grain enclosed by arsenian pyrite. Both images are from MGP-05 disk.

The alteration textures at both sites suggest oxidation. In the Masbate tailings, magnetite is replaced by hematite (martitization), and the tailings of both sites contain degraded textures, which point to chemical weathering. Pitted, porous hematite and pyrite tarnished to orange-brown in plane-polarized reflected light indicate sulfide oxidation and mineral dissolution. In tailings, the oxidation of iron sulfides is the main source of acid mine drainage (AMD) (Jambor et al. 2005), although the carbonate in the Masbate tailings (calcite in all four XRD patterns) can neutralize the acid.

In summary, the Paracale tailings contain free-milling electrum and telluride-bound gold that the SSGM process failed to recover, whereas the Masbate tailings, with little visible gold, are consistent with an efficient process for gold locked in fine sulfides.

Grain Size Composition

Figure 6 shows the particle-size curves of the Paracale (PAR-05) and Masbate (MGP-03) tailings. These were the only samples with at least 50 g of material <63 µm, which is needed for the hydrometer analysis, and so are the only ones with a complete curve.

Table S4 details the sieve results for all collected tailing samples. Although the samples may not represent the variability of the sites, they allowed a complete gradation curve including the clay and silt fractions, which strongly influence geotechnical and hydrological behavior. The Paracale tailings (PAR-05) consist of about 1.8% gravel, 76% sand, 20% silt, and 2.2% clay. About 60% of the sample lies between 0.063 and 0.25 mm (88.5% passing at 0.25 mm; 28.8% passing at 0.063 mm), that is, in the very fine to fine sand classes. The hydrometer curve levels off at 2.19% of the whole sample, indicating very little clay. The material is poorly graded: $C_u = 2.76$ is below the value of 6 required for a well-graded sand, and $C_c = 0.87$ falls below the 1.0 minimum boundary. Because $C_c < 1$, the sample lacks a smooth distribution of intermediate particles and is specifically classified as a gap-graded soil. The low C_u indicates a narrow size range, mainly fine sand to coarse silt, with the D_{10} diameter derived directly from the hydrometer curve or the finer fractions.

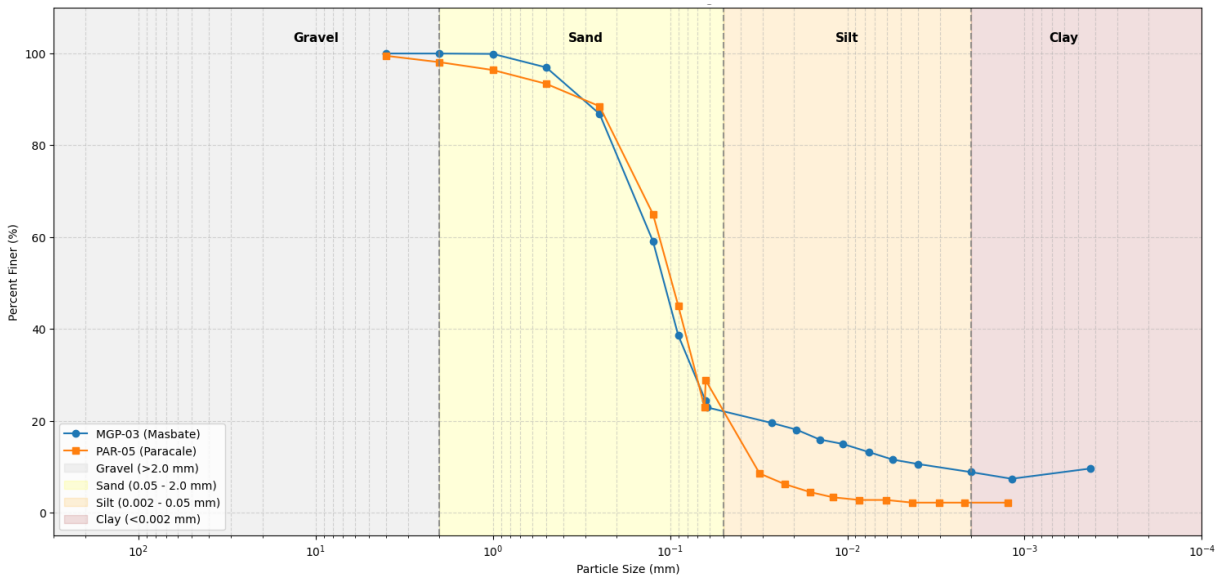


Figure 6: Particle size distribution of Paracale SSGM (PAR-05) and Masbate LSGM (MGP-03) tailings. Both tailings are mostly sand-sized, but MGP-03 has a notably higher proportion of clay-sized particles.

The Masbate tailings (MGP-03) are also sand-dominated (78% sand, 13% silt, 8.8% clay), and, as in the Paracale sample, most particles are very fine to fine sand. About 62.5% of the sample lies between 0.063 and 0.25 mm (86.8% passing at 0.25 mm; 24.3%

passing at 0.063 mm). Similar to the Paracale sample, the Masbate tailings are poorly graded and gap-graded, with computed values of C_u = 2.90 and C_c = 0.93, indicating a relatively uniform grain size. Unlike the Paracale sample, the Masbate tailings contain about 8.8% clay-sized particles. Clay-sized particles, because of their high specific surface area and electrochemical properties, can influence engineering behavior even at low concentrations (Ural 2018), and higher clay content is generally associated with a higher plasticity index and lower permeability (Qusai et al. 2025). The Masbate tailings might therefore be more plastic and less permeable than the Paracale tailings; however, this was not directly measured.

On the USDA texture triangle in **Figure 7**, the Paracale sample plots as loamy sand, while the Masbate sample plots as sandy loam. The Masbate sample has more clay (8.8% vs 2.2%) and less silt (13.2% vs 20%). LSGM plants typically use multi-stage crushing and grinding designed to maximize liberation and therefore tend to produce finer tailings (Khuduwe 2024; Quaicoe et al. 2023). SSGM operations generally use smaller ball mills (or rod mills) and simple flowsheets, and tend to produce coarser tailings because particle-size reduction is less consistent (Clemente & Lanticse 2001; Hinton et al. 2003; Samaniego & Tanchuling 2018). Despite the expected differences in the milling, the two specific samples exhibit similar overall fines content (silt plus clay) of approximately 22%.

Finer tailings can develop higher pore pressures and have lower shear strength, which increases the risk of liquefaction (Been & Li 2009; Hu et al. 2017); this would ultimately have to be tested for the Masbate TSF.

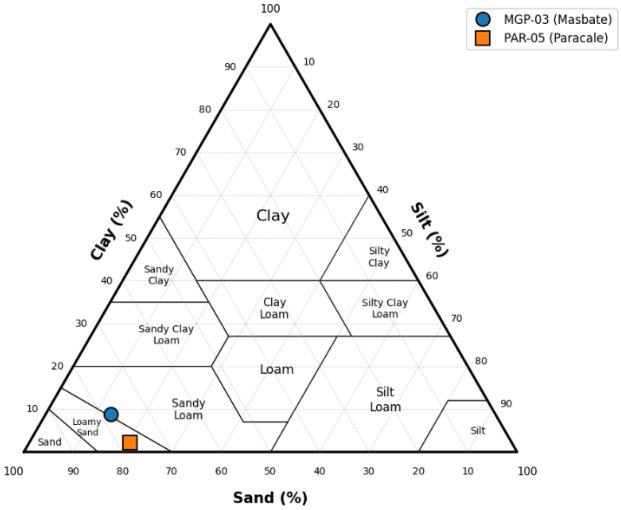


Figure 7: USDA soil texture triangle with the Paracale (PAR-05) and Masbate (MGP-03) tailings. The PAR-05 sample plots in the loamy sand field, while the MGP-03 sample plots in the sandy loam field.

Geochemical Assessment of Gangue Mineralogy

Element concentrations in the tailings, muck-outs, and low-grade ores were determined by ICP-MS and recalculated as major oxides normalized to 100% on a volatile-free basis (**Figure 8**). All samples are dominated by silicates, with SiO_2 as the most abundant oxide, followed by Fe_2O_3, Al_2O_3, CaO, MgO, and K_2O across the sample groups.

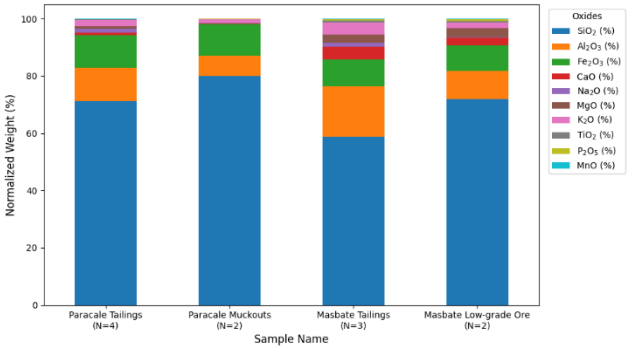


Figure 8: Major-oxide composition (wt%, normalized to 100%) of the Paracale and Masbate samples.

The Paracale tailings and muck-outs are siliceous (71.30-79.92% SiO_2), with 7.31-11.57% Al_2O_3 and 0.07-0.88% CaO. Of the major oxides, only SiO_2 is higher in the muck-outs than in the tailings; the others are lower in the muck-outs. This composition is consistent with ore from fissure-filling quartz veins, but it also contains wall-rock minerals (plagioclase, mica), so the waste is not pure vein quartz. A matrix rich in silica is likely to consume little reagent and to buffer pH weakly (Robertson & Van Staden 2009), which is favorable for leaching tests. Iron (10.80-11.32% Fe_2O_3) and the base metals (Cu, Zn, Pb) are the main constituents that could compete for lixiviant.

The composition of the Masbate samples reflects their andesitic to dioritic host rocks and bulk mining. The tailings have less silica (58.89% SiO_2) and more Al_2O_3, CaO, K_2O, MgO, and TiO_2 than the Paracale samples (71.30% SiO_2). The higher Al_2O_3 (up to 17.59%) and K_2O (up to 4.22%) in the Masbate tailings may reflect the feldspar and mica of the andesitic host rock and the alteration minerals of the deposit. The CaO (2.58-4.52%) and MgO (2.90-3.13%) probably come from calcite, plagioclase, pyroxene, chlorite, and carbonate-bearing host rock (calc-arenite of the Lanang Formation), and some CaO may also come from the lime added in the CIL circuit (Carranza 2010; Garagan et al. 2016; Johnson et al. 2025).

Most oxides are higher in the Masbate tailings than in the low-grade ore, except SiO_2, MgO, and P_2O_5. The Masbate tailings have the highest Al_2O_3 (17.59%), CaO (4.52%), TiO_2 (0.64%) and MnO (0.20%) across the Paracale and Masbate samples. This may indicate accessory apatite, rutile, or ilmenite from the host rock, which were not identified by XRD or SEM.

These compositions suggest different approaches to metal recovery. The siliceous, low-calcium Paracale matrix appears suitable for future leaching tests with green lixiviants. Silica is unlikely to consume reagents or to cause clay-swelling problems (Taheri 2023), so Fe is the main bulk competitor at the major-oxide level; Cu, Zn, and Pb are the main competitors among the trace elements (Dar et al. 2025; Li et al. 2019). The Masbate matrix may be more reagent-intensive: if all of its CaO (up to 4.52%) were present as calcite, the sample would contain at most about 8% $CaCO_3$, which could consume acid (Free 2021). This depends on the lixiviant and was not measured.

Valorization Potential of Tailings from Paracale and Masbate Mining Sites

The precious metals Au and Ag, along with the base metal Cu, were detected in the samples through ICP-MS and fire assay. These concentrations were compared against the cut-off grade of local and international mining sites to assess the valorization potential of tailings from Paracale and Masbate mining sites (Agarao 2011; Chapman et al. 2024; Johnson et al. 2025; Leal & Rankin 2022; Oceana Gold 2026; Philex Mining Corporation 2023; Riguer 2021;

Rudnick & Gao 2014; Siepka et al. 2009; Teseletso & Adachi 2022).

Figure 9 shows large differences in Au, Ag, and Cu concentrations between the two sites. To evaluate these differences, an exploratory Mann-Whitney U test was conducted across the pooled site samples (n = 6 for Paracale and n = 5 for Masbate). Because the sample sizes are small and pool tailings with muck-outs or low-grade ore, this non-parametric test is strictly exploratory. Au (median 5.35 g/t; U = 2, p = 0.017) and Ag (median 46.48 g/t; U = 1, p = 0.009) were higher in the Paracale samples than in the Masbate samples (medians 0.26 g/t Au and 0.74 g/t Ag; two-sided exact Mann-Whitney tests). The median Cu was also higher in Paracale (0.45%) than in Masbate (0.01%), and this difference was borderline (U = 3, p = 0.030). The median/mean Au of the Paracale muck-outs (1.65 g/t, range: 1.71, n = 2) is similar to that of the Masbate low-grade ore (1.22 g/t, range: 1.90, n = 2). Although MGP-04 and MGP-05 were collected from stockpiles designated as low-grade ore, one of the two grab samples contained localized sulfide-hosted electrum (2.17 g/t Au vs. 0.27 g/t Au; **Table S5**), raising the two-sample average above the typical run-of-mine mill feed grade (0.57 – 0.94 g/t Au). Both the Paracale muck-outs and the Masbate low-grade ore samples exceed the operational cut-off grades of the Masbate Gold Project, Runruno, Didipio, and Lepanto FSE (Agarao 2011; Johnson et al. 2025; Leal & Rankin 2022; Oceana Gold 2026); only the Paracale muck-outs exceed the cut-off of the Maco Mine (Riguer 2021).

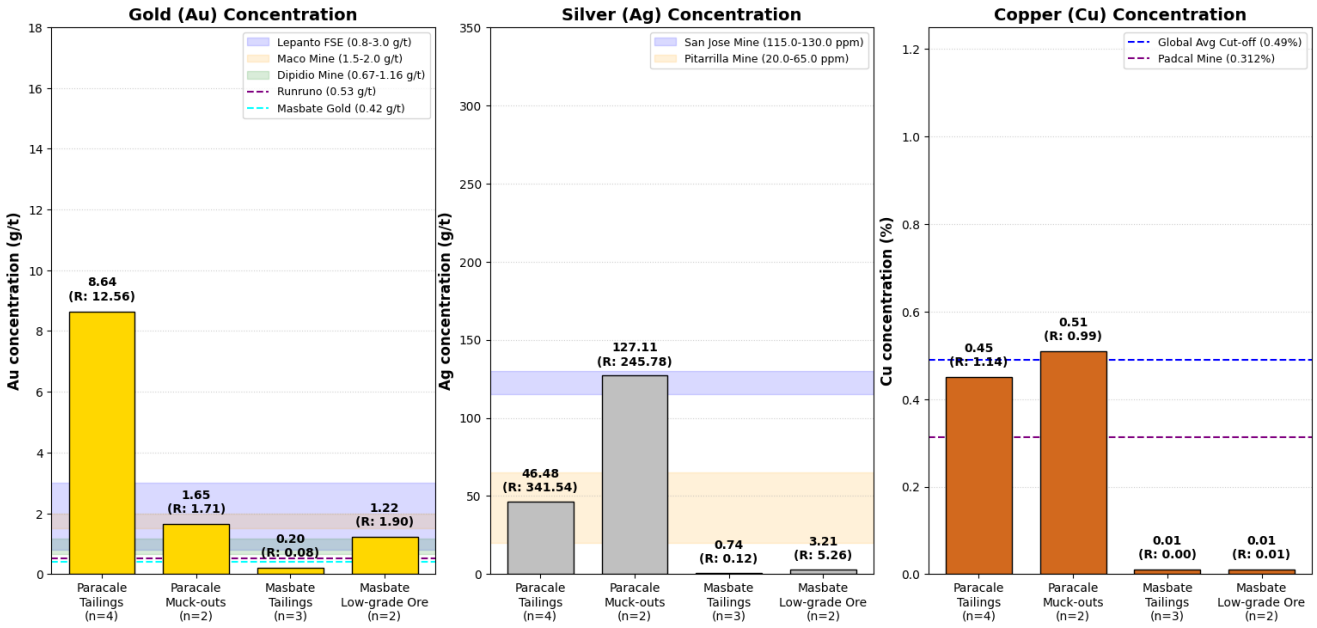


Figure 9: Gold (Au), silver (Ag), and copper (Cu) concentration per sample category vs. their mining cut-off grade (Agarao 2011; Chapman et al. 2024; Johnson et al. 2025; Leal & Rankin 2022; Oceana Gold 2026; Philex Mining Corporation 2023; Riguer 2021; Rudnick & Gao 2014; Siepka et al. 2009; Teseletso & Adachi 2022). Median values are used per sample category, and the range (R) is also shown.

The Paracale tailings (median 8.64 g/t Au; range: 12.56) are richer in gold than the muck-outs (median 1.65 g/t Au; range 1.71), which reflects the different origins of the two materials. The muck-outs may consist of broken rock, soil, clay, or low-grade waste rock excavated to reach the mineralized zones (Lee & Gu 2017), whereas the tailings are the residue of processing ROM ore (Botha et al. 2018). Overall gold recovery in Paracale is only about 27% (Gibaga et al. 2026), so the tailings retain a high gold grade (though lower than the 26.9 g/t Au mean reported from a separate Paracale pond by Gibaga et al. (2026), reflecting batch-to-batch variation in vein grades across independent sample sets). If the recovery is 27% and the tailings mass approximates the feed mass, the median grade of the ore milled would have been about 8.64/(1-0.27) = 11.84 g/t Au (or 8.37/(1-0.27) = 11.47 g/t Au based on the mean), which is characteristic of the narrow, high-grade epithermal quartz veins selectively targeted by local miners (Tharalson et al. 2019). The Masbate tailings (median 0.20 g/t Au; range: 0.08) are below all of the cut-off grades, as expected from the high recovery of the CIL circuit, whereas the Paracale tailings (median 8.64 g/t Au; range 12.56) retain a high grade, which illustrates the low recovery of traditional SSGM methods (Keane et al. 2023; Veiga et al. 2014) and indicates that the tailings deserve further evaluation as a secondary resource.

Silver is a possible co-product. The Masbate low-grade ore contains a median of 3.21 g/t Ag (range: 5.26) and its tailings 0.74 g/t Ag (range: 0.12), neither of which reaches typical cut-off grades (**Figure 9**). Paracale tailings contain silver in addition to gold. In the Philippines, silver production is associated with gold- and copper-mining operations, as reflected in national mine-level production records (Cooke et al. 2011; Mines and Geosciences Bureau 2025; Moon 2023). Because no locally applicable economic cut-off grade for silver could be identified, international benchmarks were used to contextualize the silver grades. The Paracale tailings (median 46.48 g/t Ag; range: 341.54) and muck-outs (127.11 g/t Ag; range: 245.78) exceed the cut-off grades of primary silver mines such as Pitarilla (Siepka et al. 2009) and San Jose (Chapman et al. 2024) in Mexico.

The Paracale samples show very large standard deviations, particularly for Ag (±139.13 g/t in the tailings; ±122.89 g/t in the muck-outs). Part of this variability may reflect the unsystematic dumping typical of SSGM, in which wastes go into unlined, improvised containment such as earthen ponds or concrete boxes, without blending or controlled deposition.

The variability probably has several causes. First, precious metals in the Paracale veins, such as electrum and tellurides, occur in erratic, localized high-grade clusters, which produces a nugget

effect in small samples. The Masbate deposit, also low-sulfidation epithermal, likewise has localized high-grade shoots within lower-grade envelopes.

Because SSGM recovery is only about 27%, unrecovered high-grade grains are discharged with the tailings, which preserves part of the heterogeneity of the ore. Any assessment of the secondary-resource potential of such wastes therefore needs a sampling program designed for a nuggety, heterogeneous material (larger sample masses, replicate assays, or screen fire assay).

The small number of samples (n = 4 Paracale tailings, from two ponds) also limits how well the mean and SD are estimated, despite the bulk sampling and coning and quartering. In contrast, the three Masbate tailings samples have a small SD (±0.05 g/t Ag on a mean of 0.77 g/t, a relative SD of 6.5%, against 120% for Paracale). This is consistent with fine grinding and uniform deposition reducing heterogeneity, although three samples from the perimeter of one facility cannot show homogeneity of the whole waste stream.

The Masbate samples contain little Cu (median 0.01%, range: 0.00 in tailings; median 0.01%, range: 0.01 in low-grade ore; **Figure 9**). The Paracale tailings (median 0.45% Cu, range: 1.14) and muck-outs (median 0.51% Cu, range: 0.99) reflect the Cu sulfides of the district's veins (Gibaga et al. 2026). Both exceed the Padcal cut-off of 0.31% Cu (Philex Mining Corporation 2023), while the muck-outs median (0.51% Cu) and tailings mean (0.52% Cu) slightly exceed a global average cut-off of 0.49% Cu (Teseletso & Adachi 2022). The Cu, together with Zn and Pb, means that the Paracale tailings are a complex polymetallic material in which base metals will strongly affect any leaching process. Copper can saturate the solvent (Marsden & House 2006), and the solubility of base metals in organic solvents and deep eutectic solvents (DES) varies widely (Smith et al. 2014), so Cu must be considered in future test designs for metal recovery or remediation. Relating the bulk element concentrations to their host minerals will be necessary to select and optimize extraction for this heterogeneous material.

Pollution Assessment

Ten potentially toxic elements (PTEs) were assessed: THg, Cu, Pb, As, Cd, Sb, Zn, Ni, Co, and Cr (**Table 2** and **Table 3**; complete descriptive statistics in **Table S5**). These PTEs were selected considering their potential environmental significance, association with mineralized materials, and relevance to assessing potential contaminant enrichment in mining residues. It is crucial to emphasize that this assessment is based entirely on total elemental concentrations and serves strictly to identify potential hazards; because the current work does not evaluate metal speciation, bioavailability, leachability, mobility, or specific exposure pathways, these findings should not be interpreted as a direct environmental risk assessment. Total mercury (THg), which includes elemental, inorganic, and organic Hg, was measured by DMA, and the other elements by ICP-MS.

The Paracale tailings are highly enriched relative to the upper continental crust (UCC), particularly in median THg (35.05 mg/kg, range: 96.71), Cu (0.45%, range: 1.14%), Pb (5,000.00 mg/kg, range: 4,751.90), and Zn (10,265.50 mg/kg, range: 15,782.00), which are roughly 700, 160, 295, and 150 times the UCC values (**Table S5**). The differences in Cu and Pb between the sites probably reflect the different deposits: Pb in Paracale is attributed to galena in the ores and Cu to Cu-bearing sulfides in the veins (Gibaga et al. 2026). Galena was abundant in the SEM analyses of Paracale tailings and muck-outs and Masbate tailings, making gold grains difficult to distinguish in BSE images.

Although both deposits are low-sulfidation epithermal systems, their wastes may differ in sulfide content. 'Low sulfidation' refers to the reduced state of the hydrothermal fluids and does not specify the amount of sulfide. The Masbate deposit is a shallow epithermal system with low sulfide content (commonly 1-3% or less). Because the host rocks are mined in bulk, this low sulfide content is carried into the tailings, which may explain the lower Cu and Pb (Garagan et al. 2016; Johnson et al. 2025). In Paracale, the miners selectively extract narrow, high-grade veins, so the milled ore is richer in sulfides, and the tailings inherit this. This is supported by bulk sulfur concentrations (**Table S5**), which are higher in the Paracale tailings (median 4.67% S, range: 7.97) and muck-outs (median 3.81% S, range: 2.38) than in the Masbate tailings (median 1.42% S, range: 0.64) and low-grade ore (median 2.44% S, range: 3.49).

Enrichment of As, Sb, and Cd in the wastes is likely associated with specific sulfide and sulfosalt minerals and may pose an environmental hazard. The high Zn in the Paracale tailings (median 10,265.50 mg/kg, range: 15,782.00) suggests sphalerite, which commonly contains Cd in its lattice (Kubier et al. 2019); sphalerite is therefore the probable main source of the Cd (median 107.00 mg/kg, range: 236.59). Although sphalerite was not identified in this study, the median Cd/Zn ratio of approximately 1.0% falls within the range typically reported for sphalerite and may support its presence. The Sb (median 252.90 mg/kg, range: 1,175.29 in Paracale tailings; median 2,593.81 mg/kg, range: 5,164.45 in muck-outs), which falls in the highest EF and I_{geo} classes in most sample groups, may come from tetrahedrite, a Cu-Sb sulfosalt reported from the district's veins. Arsenic is hosted by different minerals at the two sites. In Paracale, the median As (1,876.45 mg/kg, range: 6,609.40 in tailings, with a mean of 2,612.83 mg/kg that exceeds the 1,447 mg/kg reported from other local ponds by Gibaga et al. (2026) due to natural vein heterogeneity) probably comes from arsenopyrite and possibly tetrahedrite in the ore. In Masbate, the As (median 128.60 mg/kg, range: 44.20 in the tailings; median 483.80 mg/kg, range: 903.20 in the low-grade ore) is probably hosted mainly by arsenian pyrite (about 1% As), which also hosts the refractory gold.

Both sites produce wastes with high PTE concentrations, but the Paracale tailings and muck-outs contain particularly high concentrations. The median-based EF and I_{geo} classifications (**Table 2**, **Table 3,** Table **S3**) show the same pattern.

In the Paracale tailings, Paracale muck-outs, and Masbate low-grade ore, Sb falls in the highest EF category ($EF \geq 40$; **Table 2**) and the highest I_{geo} class ($I_{geo} > 5$; **Table 3**). The Paracale tailings and muck-outs both have $EF \geq 40$ for Hg, Cu, Pb, As, Cd, Sb, and Zn, and $I_{geo} > 5$ for all of these elements except Hg in the muck-outs (median 0.65 mg/kg, range: 1.06; I_{geo} Class 4; **Table 3**). The Masbate tailings have very high enrichment ($20 \leq EF < 40$) and an I_{geo} of 5 ($4 < I_{geo} \leq 5$) for As, whereas THg (median 0.74 mg/kg, range: 0.36 in tailings; median 0.35 mg/kg, range: 0.62 in low-grade ore), Sb (median 7.85 mg/kg, range: 0.93 in tailings), and Pb (median 150.90 mg/kg, range: 37.10 in tailings) are significantly enriched ($5 \leq EF < 20$) and fall in I_{geo} classes 3 to 4 ($2 < I_{geo} \leq 4$) in the tailings. In contrast, Cr, Ni, Co, and Zn in the Masbate tailings show minimal enrichment ($EF < 2$) and are uncontaminated to moderately contaminated ($I_{geo} \leq 1$; Table 2 and Table 3). Pb is below the I_{geo} threshold in the Masbate low-grade ore (median 15.90 mg/kg, range: 10.20; $I_{geo} \leq 0$) but in class 3 ($2 < I_{geo} \leq 3$) in the tailings. Since milling and cyanide leaching do not add Pb, the stockpile ore and tailings are probably not equivalent feed materials, or lead entered with a reagent or from wear, which should be investigated further. The Paracale materials are strongly enriched in Cu and Pb ($EF \geq 40$; $I_{geo} > 5$), whereas in the Masbate tailings Cu shows moderate enrichment ($2 \leq EF < 5$) and I_{geo} class 2, and Pb has EF of 5-20 and I_{geo} of 2-3 (**Table 2** and **Table 3**).

The median PTE concentrations (**Table S5**) were cross-referenced with international soil guideline values, including the Canadian Council of Ministers of the Environment (CCME; Canadian Council of Ministers of the Environment 2007), national soil limits archived in the FAOLEX database (Estonian Ministry of the Environment Regulation No. 12, cited hereafter as FAO/UN; Food and Agriculture Organization of the United Nations 2004), UNDRR/ISC hazard profiles (United Nations Office for Disaster Risk Reduction (UNDRR) & International Science Council (ISC) 2025), and thresholds reported in the literature (Hassanein 2019; Osobamiro et al. 2019; Yotova et al. 2018). International references were used because there are no national soil or sediment quality standards for PTEs in the Philippines, and comparing ponded tailings with soil guidelines provides a preliminary screening benchmark in the event of spillway overflow or land conversion.

The total concentrations in the Paracale wastes exceed several soil guideline values by large factors, which identifies a potential hazard that should be examined by leaching and exposure studies. The median As in the Paracale tailings (1,876.45 mg/kg, range: 6,609.40) is about 156 times the CCME guideline (12 mg/kg) and about 94 times the FAO/UN value (20 mg/kg) (**Figure 10**). If the As is bioavailable, chronic exposure by dust inhalation, water runoff, or uptake into crops could increase the risk of skin, lung, and bladder cancer (Palma-Lara et al. 2020; Speer et al. 2023). Cadmium in the Paracale tailings (median 107.00 mg/kg, range: 236.59) is about five times the CCME guideline (22 mg/kg) and 107 times the FAO/UN value (1 mg/kg) (**Figure 10**); Cd can cause kidney and bone damage on chronic exposure (Järup 2003; Smereczański & Brzóska 2023).

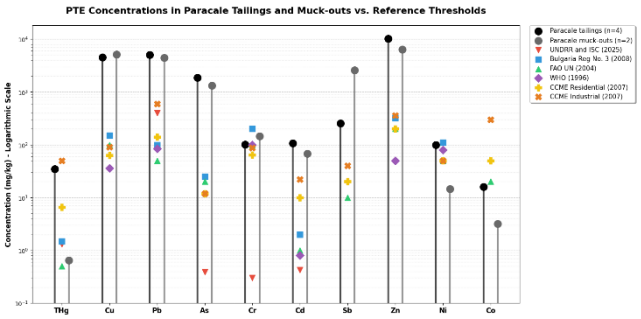


Figure 10: PTE concentrations in (A) Paracale tailings and (B) Paracale muck-outs compared with soil guideline values (Canadian Council of Ministers of the Environment 2007; Food and Agriculture Organization of the United Nations 2004; Hassanein 2019; Osobamiro et al 2019; United Nations Office for the Disaster Risk Reduction (UNDRR) & International Science Council (ISC) 2025; Yotova et al. 2018).

Median Pb is 5,000.00 mg/kg (range: 4,751.90) in the Paracale tailings and 4,427.20 mg/kg (range: 1,145.60) in the muck-outs, about 12.5 and 11 times the UNDRR value (400 mg/kg) and 8.3 and 7.4 times the CCME industrial guideline (600 mg/kg). Pb is a neurotoxin, particularly for children, and affects the cardiovascular and renal systems (Needleman 2004; Reuben 2018), if exposure pathways exist. Median THg in the Paracale tailings is 35.05 mg/kg (range: 96.71), about 27 times the UNDRR value (1.3 mg/kg) and 70 times the FAO/UN value (0.5 mg/kg). Mercury can damage the central nervous system, and leaching tests are needed to assess its mobility (Park & Zheng 2012). Median Cu (0.45%, range: 1.14%) and Zn (10,265.50 mg/kg, range: 15,782.00) in the Paracale tailings are about 45 and 51 times the FAO/UN values of 100 and 200 mg/kg, respectively (**Figure 10**). At such concentrations Cu and Zn can be phytotoxic and harm soil microbes and, if leached into surface waters, aquatic life (Gibaga et al. 2023; Wyszkowski & Brodowska 2020).

In Masbate, As is the main element of concern: a median of 483.80 mg/kg (range: 903.20) in the low-grade ore and 128.60 mg/kg (range: 44.20) in the tailings, about 40 and 11 times the CCME guideline of 12 mg/kg (**Figure 11**). If the tailings weather and the As is mobilized, it could leach into groundwater and affect drinking water (Smedley & Kinniburgh 2002). The engineered Masbate TSF may help limit contaminant release, although its design alone does not establish lower environmental risk. Calcite in the tailings may reduce the mobility of some metals by buffering acidity. However, the resulting increase in pH may also promote arsenic mobilization as arsenate (Dixit & Hering 2003; Noble & Lottermoser 2012). Sb in the low-grade ore (median 24.94 mg/kg, range: 26.18) is slightly above the CCME guideline (20 mg/kg), whereas Cr in the Masbate tailings (median 36.00 mg/kg, range: 8.00) is below the guideline (**Figure 11**). The high concentrations suggest that land around the sampled Paracale tailings may be unsuitable for residential, agricultural, or unprotected industrial use unless it is assessed, whereas the Masbate site may require groundwater monitoring and containment to keep the As from reaching aquifers. These results describe only the materials sampled. Because the samples are few, they do not represent the wider Paracale and Masbate districts, and further sampling and testing are needed before regional conclusions are drawn.

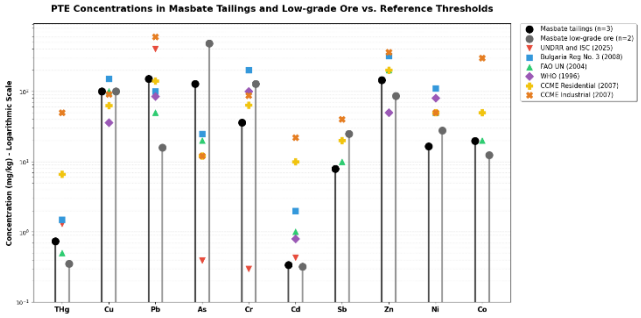


Figure 11: PTE concentrations in the Masbate tailings and low-grade ore compared with soil guideline values (Canadian Council of Ministers of the Environment 2007; Food and Agriculture Organization of the United Nations 2004; Hassanein 2019; Osobamiro et al. 2019; United Nations Office for the Disaster Risk Reduction (UNDRR) & International Science Council (ISC) 2025; Yotova et al. 2018)

CONCLUSION

This study compares the composition and mineralogy of wastes from one small-scale site (Paracale) and one large-scale operation (Masbate). Because deposit geology and operating scale differ together, their effects cannot be separated. The Paracale wastes come from selectively mined quartz veins treated by amalgamation, and the Masbate wastes from bulk-mined, calcite-bearing volcaniclastics treated by cyanide leaching. These differences are associated with different waste compositions and recovery potential.

Because recovery at Paracale is low, the tailings retain high metal grades (median 8.64 g/t Au, range: 12.56; 46.48 g/t Ag, range: 341.54; and 0.45% Cu, range: 1.14) in a siliceous matrix (71.30-79.92% SiO_2) and may be a secondary resource. The silica-rich gangue should consume little reagent and is a reasonable starting material for tests with green lixiviants such as deep eutectic solvents (DES), although Cu, Zn, Pb, and Fe may compete for the lixiviant. The Paracale tailings contain liberated electrum, some of which reacted with mercury to form Au-Ag-Hg particles, as well as electrum enclosed in quartz and Au-Ag tellurides. Uraninite enriched in Y and Dy (Figure S1) and Ce-dominant monazite (Figure S2) were also found as accessory minerals. While bulk U and Th concentrations in the tailings (median 1.11 mg/kg U; 0.96 mg/kg Th; **Table S5**) remain within normal crustal levels, the presence of discrete uraninite and monazite grains indicates that

heavy mineral fractions should be monitored for radionuclide partitioning during secondary processing.

In contrast, the Masbate tailings contain little gold (median 0.20 g/t Au; range: 0.08) and silver (median 0.74 g/t Ag; range: 0.12) and are not a target for precious-metal recovery. The Masbate matrix is aluminosilicate-rich with up to 4.52% CaO and may therefore consume acid during leaching; this was not tested. In the low-grade ore, gold occurs in arsenian pyrite and pyrite (**Figure 5**). The Masbate samples also contain REE-bearing minerals, including REE-Ti phosphate and monazite (**Figure S3**). As at Paracale, these are mineralogical occurrences only, and quantitative sampling is needed to assess them.

The two sites may need different management. The total concentrations of Hg, Pb, As, Cd, Cu, and Zn in the Paracale wastes exceed soil guideline values by large factors, which identifies a potential hazard. This represents a preliminary identification of potential hazards rather than a direct environmental risk assessment. Health outcomes and metal mobility depend on speciation, leachability, and bioavailability, which should be studied next. The Paracale wastes are candidates for tests of combined decontamination and metal recovery, and the Masbate tailings may need groundwater monitoring and containment because of their arsenic content. Because few samples were collected, the results are preliminary; broader sampling and testing are needed before conclusions are drawn for the Paracale and Masbate districts. Future work should include (i) replicate, depth-resolved sampling of the ponds, (ii) leaching and acid-base accounting tests, (iii) local-background soils and sediments, and (iv) radiochemical activity measurements to assess potential radionuclide concentration during mineral separation.

ACKNOWLEDGMENTS

This paper was published through the following research projects funded by PCIEERD-GIA and DOST-GIA: (1) Application of Ionometallurgy for the Recovery and Extraction of Copper from Copper Ore and Artisanal Copper-Gold Tailings (i-REACT), Project No. 11306; and (2) NEAT-ORE: Novel Extraction of Au and Other Critical Metals in Artisanal Tailings and Low-Grade Ores Using Novel Organic Solvents - Phase I, Project No. 1212066. We also gratefully acknowledge the following contributions: the small-scale and large-scale mining cooperatives and the mining company for granting access to their sites and permitting sample collection; the National Institute of Geological Sciences for providing facilities and enabling hands-on XRD analysis; and Prof. Gawen Jenkin and Dr. Leon Hicks of the School of Geography, Geology and the Environment, University of Leicester, for providing laboratory access and assistance with the QEMSEM analysis.

CONFLICT OF INTEREST

The authors declare that there is no conflict of interest.

CONTRIBUTIONS OF INDIVIDUAL AUTHORS

CRediT Roles: **John Henry C. Gervasio**: Conceptualization, Methodology, Formal analysis, Investigation, Data Curation, Writing – Original Draft, Visualization, Project administration; **Alexandria M. Tanciongco**: Conceptualization, Methodology, Formal analysis, Investigation, Data Curation, Writing – Original Draft, Visualization, Funding Acquisition; **Rico Neil M. Quierrez**: Conceptualization, Methodology, Investigation, Writing – Review & Editing; **Jessa Mae V. Estoque**: Investigation, Writing – Review & Editing, Project administration; **Katrina Mae S. Flores**: Investigation, Writing – Review & Editing, Project administration; **Angel T. Bautista VII**: Resources, Writing – Review & Editing, Supervision; **Cris Reven L. Gibaga**: Conceptualization, Writing – Original Draft, Writing – Review & Editing, Supervision; **Jessie O. Samaniego**: Resources, Writing – Review & Editing, Supervision.

REFERENCES

Agarao, M. (2011). *Lepanto Conso. Mining Co. (LC/B)*. https://www.philequity.net/uploadedfile/20111207172453420_Lepanto%20Consolidated%20Mining%20report.pdf

Aglibot, J. M. B., Tanciongco, A. M., Quierrez, R. N. M., Gervasio, J. H. C., Rasay, A. F. P., Acampado, J. B., Peregrino, F. R. A., Estoque, J. M. V., & Samaniego, J. O. (2025). Pollution assessment and mercury leaching using environmentally friendly solvents from small-scale gold mine wastes in Camarines Norte. *Journal of Degraded and Mining Lands Management*, *12*(4), 8139–8147. https://doi.org/10.15243/jdmlm.2025.124.8139

Ali, A., Chiang, Y. W., & Santos, R. M. (2022). X-ray Diffraction Techniques for Mineral Characterization: A Review for Engineers of the Fundamentals, Applications, and Research Directions. *Minerals*, *12*(2), 205. https://doi.org/10.3390/min12020205

ASTM International. (2017). Standard Practice for Classification of Soils for Engineering Purposes (Unified Soil Classification System) (ASTM D2487-17).

ASTM International. https://doi.org/10.1520/D2487-17 ASTM International. (2021). Standard Test Methods for Particle-Size Distribution (Gradation) of Soils Using Sieve Analysis (ASTM D6913/D6913M-17).

ASTM International. https://doi.org/10.1520/D6913_D6913M-17 ASTM International. (2021). Standard Test Method for Particle-Size Distribution (Gradation) of Fine-Grained Soils Using the Sedimentation (Hydrometer) Analysis (ASTM D7928-21e1). ASTM International. https://doi.org/10.1520/D7928-21E01

Baláž, P. (2008). Mechanochemistry in Minerals Engineering. In P. Baláž (Ed.), *Mechanochemistry in Nanoscience and Minerals Engineering* (pp. 257–296). Springer. https://doi.org/10.1007/978-3-540-74855-7_5

Bautista, C. P., Punzalan, J., Samaniego, J., Gibaga, C. R., Tanciongco, A., Quierrez, R. N., Gervasio, J. H., & Reyes, R. C. (2024). Pollution Assessment of Potentially Toxic Elements in Marine Sediment from Puerto Princesa Bay, Palawan, the Philippines. *Philippine Journal of Science*, *153*(2). https://doi.org/10.56899/153.02.02

Been, K., & Li, A. L. (2009). *Soil Liquefaction and Paste Tailings* (R. Jewell, A. B. Fourie, S. Barrera, & J. Wiertz, Eds.; pp. 281–290). Australian Centre for Geomechanics. Paste 2009: Twelfth International Seminar on Paste and Thickened Tailings, 2009 21-24 April, Viña del Mar. https://doi.org/10.36487/ACG_repo/963_32

Bhandari, B. P., & Dhakal, S. (2021). A multidisciplinary approach of landslide characterization: A case of the Siwalik zone of Nepal

Himalaya. *Journal of Asian Earth Sciences: X*, *5*, 100061. https://doi.org/10.1016/j.jaesx.2021.100061

Botha, S., le Roux, J. D., & Craig, I. K. (2018). Hybrid non-linear model predictive control of a run-of-mine ore grinding mill circuit. *Minerals Engineering*, *123*, 49–62. https://doi.org/10.1016/j.mineng.2018.04.016

Buat-Menard, P., & Chesselet, R. (1979). Variable influence of the atmospheric flux on the trace metal chemistry of oceanic suspended matter. *Earth and Planetary Science Letters*, *42*(3), 399–411. https://doi.org/10.1016/0012-821X(79)90049-9

Bunye, P. (2018, July 18). *Mining in the Philippines*. Lexology. https://www.lexology.com/library/detail.aspx?g=7537d507-42c3-4274-bd2a-d66507c629d6

Cacciuttolo, C., Guzmán, V., Catriñir, P., & Atencio, E. (2024). Sensor Technologies for Safety Monitoring in Mine Tailings Storage Facilities: Solutions in the Industry 4.0 Era. *Minerals*, *14*(5), 446. https://doi.org/10.3390/min14050446

Canadian Council of Ministers of the Environment. (2007). *Canadian Soil Quality Guidelines for the Protection of Environmental and Human Health*. Environment Canada. https://support.esdat.net/Environmental%20Standards/canada/soil/rev_soil_summary_tbl_7.0_e.pdf

Carranza, E. J. M. (2010). Catchment basin modelling of stream sediment anomalies revisited: Incorporation of EDA and fractal analysis. *Geochemistry: Exploration, Environment, Analysis*, *10*(4), 365–381. https://doi.org/10.1144/1467-7873/09-224

Castroviejo, R. (2023). *A Practical Guide to Ore Microscopy: Ore Textures and Automated Ore Analysis* (Vol. 2). Springer Nature.

Casulla, M. A. A., & Mizunaga, H. (2023). Characterization of potential Cu-Au mineralization using electrical resistivity and induced polarization methods: A case study in Eastern Labo, Bicol, Philippines. *Journal of Geophysics and Engineering*, *20*(2), 411–425. https://doi.org/10.1093/jge/gxad018

Chapman, E., Weedon, P., Espinoza, R., Veillette, M., & Gonzales, P. (2024). *Fortuna Silver Mines Inc.: San Jose Mine, Oaxaca, Mexico Technical Report Effective Date: December 31, 2023*. https://minedocs.com/26/San-Jose-TR-12312023.pdf

Clemente, E., & Lanticse, L. J. (2001). Small-scale gold mining operations in Benguet and Camarines Norte, Philippines. *Philippine Engineering Journal*, *22*(1), 55–68.

Cooke, D., Hollings, P., & Chang, Z. (2011). Exploration Tools for Linked Porphyry and Epithermal Deposits: Example from the Mankayan Intrusion-Centered Cu-Au District, Luzon, Philippines. *Economic Geology*, *106*, 1365–1398. https://doi.org/10.2113/econgeo.106.8.1365

Craig, J. R., & Vaughan, D. J. (1994). *Ore Microscopy and Ore Petrography* (2nd ed.). John Wiley & Sons, Inc.

Dar, A. A., Chen, Z., Zhang, G., Hu, J., Zaghib, K., Deng, S., Wang, X., Haghighat, F., Mulligan, C. N., An, C., Ramirez, A. A., & Sun, S. (2025). Sustainable Extraction of Critical Minerals from Waste Batteries: A Green Solvent Approach in Resource Recovery. *Batteries*, *11*(2), 51. https://doi.org/10.3390/batteries11020051

Deiss, R. S. (2025). *Geotechnical characterization of Nalunaq Gold Mine residues for in- situ engineering applications*. 72 [Master's thesis, Technical University of Denmark]

dela Cruz, K. M. T. D., Madayag, J. A. T., Arpa, M. C. B., Samaniego, J. O., Peregrino, F. R. A., Quierrez, R. N. M., & Tanciongco, A. M. (2025). Pollution assessment and mercury speciation of small-scale gold mine (SSGM) tailings, sediments, and ore from Camarines Norte, Philippines. *Journal of Degraded and Mining Lands Management*, *12*(4), 8023–8034. https://doi.org/10.15243/jdmlm.2025.124.8023

Dixit, S., & Hering, J. G. (2003). Comparison of Arsenic(V) and Arsenic(III) Sorption onto Iron Oxide Minerals: Implications for Arsenic Mobility. *Environmental Science & Technology*, *37*(18), 4182–4189. https://doi.org/10.1021/es030309t

Eberle, A., Garbowski, T., & Nickell, S. (2017). *ZEISS MultiSEM Sample Preparation Guide*. https://doi.org/10.13140/RG.2.2.33956.78726

Filminera Resources Corp. (2018). *Project Description for Scoping—Masbate Gold Project Processing Plant Expansion*.

Food and Agriculture Organization of the United Nations. (2004). *Maximum Limits for Dangerous Substances in Soil and Groundwater—Regulation of the Minister of the Environment No. 12 of 2 April 2004*. https://faolex.fao.org/docs/pdf/est97999E.pdf

Free, M. L. (2021). *Hydrometallurgy: Fundamentals and Applications*. Springer Nature.

Gabo-Ratio, J., Buena, A., Villaplaza, B. R., Payot, B., Dimalanta, C., Queaño, K., Andal, E., & Yumul, G. P., Jr. (2020). Epithermal mineralization of the Bonanza-Sandy vein system, Masara Gold District, Mindanao, Philippines. *Journal of Asian Earth Sciences: X*, *4*, 100041. https://doi.org/10.1016/j.jaesx.2020.100041

Garagan, T., Pemberton, K., Jones, K., & Rajala, J. (2016). *B2 Gold Masbate Gold Operation NI 43-101 Technical Report on Operations* (Technical Report Nos. 43–101). https://s204.q4cdn.com/324791784/files/doc_downloads/2025/10/22/Masbate-Technical-Report-December-31-2016.pdf#:~:text=The%20process%20plant%20is%20a%20conventional%20carbon%2Din%2Dleach,A%202.1%20km%20long%2C%20630%20mm%20operative

Gibaga, C. R. L., Samaniego, J. O., Tanciongco, A. M., & Quierrez, R. N. M. (2023). Pollution assessment of mercury and other potentially toxic elements in the marine sediments of Mambulao Bay, Jose Panganiban, Camarines Norte, Philippines. *Marine Pollution Bulletin*, *192*, 115032. https://doi.org/10.1016/j.marpolbul.2023.115032

Gibaga, C. R. L., Samaniego, J. O., Tanciongco, A. M., Quierrez, R. N. M., Gervasio, J. H. C., & Bautista VII, A. T. (2026). Environmental risks and resource potential in small-scale gold mine tailings: A case study of Camarines Norte and Benguet, Philippines. *Journal of Degraded and Mining Lands Management*, *13*(3), 10787–10798. https://doi.org/10.15243/jdmlm.2026.133.10787

Gibaga, C. R., Samaniego, J., Tanciongco, A., Quierrez, R. N., Montano, M., Gervasio, J. H., Reyes, R., & Peralta, M. (2022). Pollution and radiological risk assessments of mine wastes from selected legacy and active mines in the Philippines. *Journal of*

Degraded and Mining Lands Management, *9*, 3621. https://doi.org/10.15243/jdmlm.2022.094.3621

Giese, U., Knittel, U., & Kramm, U. (1986). The Paracale Intrusion: Geologic setting and petrogenesis of a trondhjemite intrusion in the Philippine Island Arc. *Journal of Southeast Asian Earth Sciences*, *1*(4), 235–245. https://doi.org/10.1016/0743-9547(86)90018-8

Goodall, W. R., Scales, P. J., & Butcher, A. R. (2005). The use of QEMSCAN and diagnostic leaching in the characterisation of visible gold in complex ores. *Minerals Engineering, Selected Papers from Precious Metals '04, Cape Town, South Africa, November 2004*, *18*(8), 877–886. https://doi.org/10.1016/j.mineng.2005.01.018

Hassanein, K. (2019). Chemical analysis and environmental impact of heavy metals in soil of Wadi Jazan Area, Southwest of Saudi Arabia. *Applied Ecology and Environmental Research*, *17*, 7067–7083. https://doi.org/10.15666/aeer/1703_70677084

Hinton, J. J., Veiga, M. M., & Veiga, A. T. C. (2003). Clean artisanal gold mining: A utopian approach? *Journal of Cleaner Production, Environmental Management*, *11*(2), 99–115. https://doi.org/10.1016/S0959-6526(02)00031-8

Hossain, M. S., Islam, M. A., Badhon, F. F., & Imtiaz, T. (2021a). *Hydrometer Analysis*. https://uta.pressbooks.pub/soilmechanics/chapter/hydrometer-analysis/

Hossain, M. S., Islam, M. A., Badhon, F. F., & Imtiaz, T. (2021b). *Sieve Analysis*. https://uta.pressbooks.pub/soilmechanics/chapter/sieve-analysis/

Hu, L., Wu, H., Zhang, L., Zhang, P., & Wen, Q. (2017). Geotechnical Properties of Mine Tailings. *Journal of Materials in Civil Engineering*, *29*(2), 04016220. https://doi.org/10.1061/(ASCE)MT.1943-5533.0001736

Ineson, P. R. (1989). *Introduction to Practical Ore Microscopy*. Routledge.

Jambor, J., Ptacek, C., Blowes, D., & Moncur, M. (2005). Acid drainage from the oxidation of iron sulfides and sphalerite in mine wastes. *Proceedings of Lead & Zinc 5*, 715–737.

James, L. P., & Fuchs, W. A. (1990). Exploration of the Exciban gold-copper-tellurium vein system, Camarines Norte, Philippines. *Journal of Geochemical Exploration*, *35*(1), 363–385. https://doi.org/10.1016/0375-6742(90)90044-B

Järup, L. (2003). Hazards of heavy metal contamination. *British Medical Bulletin*, *68*(1), 167–182. https://doi.org/10.1093/bmb/ldg032

Jenkin, G. R. T., Arcilla, C. A., Abbott, A. P., Bateson, L., Bautista VII, A. T., Chambers, J. E., Devanadera, M. C., Duddigan, S., Fernando, E. S., Gervasio, J. H. C., Gibaga, C., Lazaro, J. E. H., Menor, T. L. F., Naden, J., Newsome, L., Pan, Y., Quierrez, R. N. M., Quimado, M. O., Samaniego, J. O., … Yan, Y. (2024). *Recent developments in the science and technology of in situ solvent leaching of tailings for reprocessing, rehabilitation and closure*. 29–44. https://doi.org/10.36487/ACG_repo/2415_0.03

Johnson, M., Montano, P., Rajala, J., & Jones, K. (2025). B2 Gold Masbate Gold Project Philippines NI 43-101 Technical Report. *Technical Report*. https://s204.q4cdn.com/324791784/files/doc_downloads/2025/11/13/Masbate-2025-Final-7Nov2025.pdf

Kalore, S. A., & Sivakumar Babu, G. L. (2023). Significance of *Cu* and *Cc* in Evaluating Internal Stability with Application to Design of Subbase Gradation in Pavements. *Transportation Geotechnics*, *40*, 100972. https://doi.org/10.1016/j.trgeo.2023.100972

Keane, S., Bernaudat, L., Davis, K. J., Stylo, M., Mutemeri, N., Singo, P., Twala, P., Mutemeri, I., Nakafeero, A., & Etui, I. D. (2023). Mercury and artisanal and small-scale gold mining: Review of global use estimates and considerations for promoting mercury-free alternatives. *Ambio*, *52*(5), 833–852. https://doi.org/10.1007/s13280-023-01843-2

Kerr, P. F. (1977). *Optical Mineralogy*. McGraw-Hill.

Khuduwe, M. J. (2024). *Extraction of Gold From Tailings Using Environmentally Friendly Reagents* [M.S.Eng., University of the Witwatersrand, Johannesburg (South Africa)]. https://www.proquest.com/docview/3258406187/abstract/6B2D1DC2487246A9PQ/1

Kleeberg, R., Monecke, T., & Hillier, S. (2008). Preferred orientation of mineral grains in sample mounts for quantitative XRD measurements: How random are powder samples? *Clays and Clay Minerals*, *56*(4), 404–415. https://doi.org/10.1346/CCMN.2008.0560402

Kubier, A., Wilkin, R. T., & Pichler, T. (2019). Cadmium in soils and groundwater: A review. *Applied Geochemistry*, *108*, 104388. https://doi.org/10.1016/j.apgeochem.2019.104388

Leal, V., & Rankin, R. (2022). *Metals Exploration PLC: Updated Mineral Resource and Ore Reserve Estimate*. https://metalsexploration.com/wp-content/uploads/2022/02/Updated-Mineral-Resource-and-Ore-Reserve-Estimate-5072B.pdf

Lee, C., & Gu, F. (2017). *Co-disposal of waste rock with backfill* (M. Hudyma & Y. Potvin, Eds.; pp. 353–362). Australian Centre for Geomechanics. UMT 2017: First International Conference on Underground Mining Technology, 2017 11-13 October, Sudbury. https://doi.org/10.36487/ACG_rep/1710_27_Lee

Li, B., Wei, Y., Wang, H., Yang, Y., & Yin, Y. (2019). Preparation of ZnSO4·7H2O and Separation of Zinc from Blast Furnace Sludge by Leaching-Purification-Crystallization Method. *ISIJ International*, *59*(1), 201–207. https://doi.org/10.2355/isijinternational.ISIJINT-2018-401

Louvel, M., Etschmann, B., Guan, Q., Testemale, D., & Brugger, J. (2022). Carbonate complexation enhances hydrothermal transport of rare earth elements in alkaline fluids. *Nature Communications*, *13*(1), 1456. https://doi.org/10.1038/s41467-022-28943-z

Marsden, J., & House, I. (2006). *The Chemistry of Gold Extraction*. SME.

Mines and Geosciences Bureau. (2010). *Geology of the Philippines* (2nd ed.). Mines and Geosciences Bureau.

https://dokumen.pub/qdownload/geology-of-the-philippines-2nd-edition-2nbsped.html

Mines and Geosciences Bureau. (2025). *Mining Industry Statistics*. Mines and Geosciences Bureau. https://mgb.gov.ph/images/Mineral_Statistics/2025/2024MISasofMAR112025final_for_posting.pdf

Mitchell, A. H. G., & Balce, G. R. (1990). Geological features of some epithermal gold systems, Philippines. *Journal of Geochemical Exploration*, *35*(1), 241–296. https://doi.org/10.1016/0375-6742(90)90041-8

Mitchell, A. H. G., & Carlile, J. C. (1994). Mineralization, antiforms and crustal extension in andesitic arcs. *Geological Magazine*, *131*(2), 231–242. https://doi.org/10.1017/S001675680001075X

Moon, J. W. (2023). *2019 Minerals Yearbook* (Vol. 3). U.S. Geological Survey. https://doi.org/10.3133/70178411.

Müller, G. (1969). *Index of geoaccumulation in sediments of the Rhine River*. 108–118.

National Economic Development Authority, Department of Environment and Natural Resources, Department of Finance, & Development Academy of the Philippines. (2022). *Review of Philippines Large-Scale Metallic Mines* (p. 96).

Ndikumana, J., Kashinga, R. J., Kumaran, G. S., & Langi, E. (2024). An Investigation of the Mechanical and Durability Properties of Hollow Concrete Blocks Made with Copper Mine Tailings as a Partial Cement Replacement. *Advanced Engineering Forum*, *52*, 11–26. https://doi.org/10.4028/p-WC6eo6

Needleman, H. (2004). Lead Poisoning. *Annual Review of Medicine*, *55*(Volume 55, 2004), 209–222. https://doi.org/10.1146/annurev.med.55.091902.103653

Nesse, W. D. (2020). *Introduction to Optical Mineralogy* (4th ed). Oxford University Press.

Noble, T. L., & Lottermoser, B. G. (2012). *Evaluating the remediation of arsenic-rich tailings at the historic Royal George tin mine, Tasmania, Australia* (A. B. Fourie & M. Tibbett, Eds.; pp. 163–172). Australian Centre for Geomechanics. Mine Closure 2012: Seventh International Conference on Mine Closure, 2012 25-27 September, Brisbane. https://doi.org/10.36487/ACG_rep/1208_16_Noble

Oceana Gold. (2026). *Annual Information Form for the year ended December 31, 2025*. https://minedocs.com/31/OceanaGold-AIF-12312025.pdf

Osobamiro, T., Awolesi, O., Alabi, O., Oshinowo, A., Idris, M., & Busari, F. (2019). Heavy Metal Levels of Soil Samples Collected From a Major Industrial Area in Abeokuta, Southwestern Nigeria. *Indian Journal of Scientific Research*, *9*, 914–919. https://doi.org/10.29322/IJSRP.9.08.2019.p92125

Palma-Lara, I., Martínez-Castillo, M., Quintana-Pérez, J. C., Arellano-Mendoza, M. G., Tamay-Cach, F., Valenzuela-Limón, O. L., García-Montalvo, E. A., & Hernández-Zavala, A. (2020). Arsenic exposure: A public health problem leading to several cancers. *Regulatory Toxicology and Pharmacology*, *110*, 104539. https://doi.org/10.1016/j.yrtph.2019.104539

Park, J.-D., & Zheng, W. (2012). Human Exposure and Health Effects of Inorganic and Elemental Mercury. *Journal of Preventive Medicine and Public Health*, *45*(6), 344–352. https://doi.org/10.3961/jpmph.2012.45.6.344

Philex Mining Corporation. (2023). *Padcal—Philex Mining Corporation*. https://www.philexmining.com.ph/padcal

Pracejus, B. (2015). *The Ore Minerals under the Microscope* (2nd ed.). Elsevier.

Putra, B., Surachman, M., Darmawan, I., Fanindi, A., Sawen, D., Dianita, R., Praptiwi, I., Sawo, K., Hambakodu, M., Hariadi, B., Koten, B., Akhadiarto, S., Bahar, S., Sirait, J., Nulik, J., Simanihuruk, K., Gopar, R., & Suharlina, S. (2024). Assessing phytoremediation strategies for gold mine tailings: A bibliometric and systemic review. *Environmental Geochemistry and Health*, *47*. https://doi.org/10.1007/s10653-024-02317-4

Quaicoe, I., Beyuo, M., Quaicoe, S., & Lasidzi, N. A. (2023). Diagnostic gold deportment studies and leaching behaviour of small-scale gold mining tailings from Eastern Region, Ghana. *Journal of Sustainable Mining*, *22*(2), 81–88. https://doi.org/10.46873/2300-3960.1375

Qusai, A., Szendefy, J., & Vásárhelyi, B. (2025). Effect of Changing Sand Content on Liquid Limit and Plasticity Index of Clay. *Geotechnics*, *5*(1), 4. https://doi.org/10.3390/geotechnics5010004

Reimann, C., & Caritat, P. D. (2000). Intrinsic Flaws of Element Enrichment Factors (EFs) in Environmental Geochemistry. *Environmental Science & Technology*, *34*(24), 5084–5091. https://doi.org/10.1021/es001339o

Reuben, A. (2018). Childhood Lead Exposure and Adult Neurodegenerative Disease. *Journal of Alzheimer's Disease*, *64*(1), 17–42. https://doi.org/10.3233/JAD-180267

Riguer, D. E. (2021). *Technical Report on the Exploration Results and Mineral Resource Estimate of the Maco Gold Mine Located in Maco and Mabini Municipalities, Davao de Oro Province, Philippines*. https://www.apexmines.com/wp-content/uploads/2021/07/2021_MPSA-234_Mineral_Resource_Update_Apex.pdf

Robertson, S. W., & Van Staden, P. J. (2009). The progression of metallurgical testwork during heap leach design. *The Southern African Institute of Mining and Metallurgy*, 31–42. https://www.saimm.co.za/Conferences/Hydro2009/031-042_Robertson.pdf

Rudnick, R., & Gao, S. (2014). Composition of the Continental Crust. *Treatise on Geochemistry*, *3*, 1–64. https://doi.org/10.1016/B0-08-043751-6/03016-4

Sajona, F. G., & Maury, R. C. (1998). Association of adakites with gold and copper mineralization in the Philippines. *Comptes Rendus de l'Académie Des Sciences - Series IIA - Earth and Planetary Science*, *326*(1), 27–34. https://doi.org/10.1016/S1251-8050(97)83200-4

Samaniego, J., Gibaga, C. R., Tanciongco, A., & Rastrullo, R. (2020). Total Mercury in Soils and Sediments in the Vicinity of Abandoned Mercury Mine Area in Puerto Princesa City,

Philippines. *Applied Sciences*, *10*(13), 4599. https://doi.org/10.3390/app10134599

Samaniego, J. O., & Tanchuling, M. A. N. (2018). Physico-chemical Characteristics of Wastewater from a Ball Mill Facility in Small-Scale Gold Mining Area of Paracale, Camarines Norte, Philippines. *Philippine Journal of Science*, *147*(3), 343–356.

Seward, T. M., Williams-Jones, A. E., & Migdisov, A. A. (2014). *13.2-The chemistry of metal transport and deposition by ore-forming hydrothermal fluids* (2nd ed.). Elsevier Ltd. https://doi.org/http://dx.doi.org/10.1016/B978-0-08-095975-7.01102-5

Siepka, A., Robertson, J., & Wells, P. (2009). *Silver Standard Resources Inc. NI 43-101 Technical Report—Pitarrilla Property Pre-feasibility Study* (Nos. 0853750400-REP-R0002-03). Wardrop. https://www.ssrmining.com/assets/pdfs/Pitarrilla_Sep_21_rev.pdf

Sillitoe, R. H. (1991). Intrusion-related gold deposits. In R. P. Foster (Ed.), *Gold metallogeny and exploration* (pp. 165–209). Springer US. https://doi.org/10.1007/978-1-4613-0497-5_6

Smedley, P. L., & Kinniburgh, D. G. (2002). A review of the source, behaviour and distribution of arsenic in natural waters. *Applied Geochemistry*, *17*(5), 517–568. https://doi.org/10.1016/S0883-2927(02)00018-5

Smereczański, N. M., & Brzóska, M. M. (2023). Current Levels of Environmental Exposure to Cadmium in Industrialized Countries as a Risk Factor for Kidney Damage in the General Population: A Comprehensive Review of Available Data. *International Journal of Molecular Sciences*, *24*(9), 8413. https://doi.org/10.3390/ijms24098413

Smith, E. L., Abbott, A. P., & Ryder, K. S. (2014). Deep Eutectic Solvents (DESs) and Their Applications. *Chemical Reviews*, *114*(21), 11060–11082. https://doi.org/10.1021/cr300162p

Speer, R., Zhou, X., Volk, L., Liu, K. J., & Hudson, L. (2023). Arsenic and cancer: Evidence and mechanisms. In *Advances in Pharmacology* (Vol. 96, pp. 151–202). Academic Press. https://doi.org/10.1016/bs.apha.2022.08.001

Spry, P., & Gedlinske, B. (1987). *Tables for the Determination of Common Opaque Minerals*.

Sutherland, R. A. (2000). Bed sediment-associated trace metals in an urban stream, Oahu, Hawaii. *Environmental Geology*, *39*(6), 611–627. https://doi.org/10.1007/s002540050473

Taheri, B. (2023). Iron removal from kaolin by oxalic acid using a novel pre-agitating and high-pressure washing technique. *Clay Minerals*, *58*(2), 224–233. https://doi.org/10.1180/clm.2023.11

Tan, Ma. G. R., Sanoy, J. R., & Junio-Jimenez, J. (2025). Durability Assessment of Loadbearing Concrete Hollow Blocks with Gold Mine Tailings as a Partial Substitute for Sand. *IOP Conference Series: Earth and Environmental Science*, *1546*(1), 012053. https://doi.org/10.1088/1755-1315/1546/1/012053

Teseletso, L. S., & Adachi, T. (2022). Long-Term Sustainability of Copper and Iron Based on a System Dynamics Model. *Resources*, *11*(4), 37. https://doi.org/10.3390/resources11040037

Tharalson, E. R., Monecke, T., Reynolds, T. J., Zeeck, L., Pfaff, K., & Kelly, N. M. (2019). The Distribution of Precious Metals in High-Grade Banded Quartz Veins from Low-Sulfidation Epithermal Deposits: Constraints from µXRF Mapping. *Minerals*, *9*(12), 740. https://doi.org/10.3390/min9120740

Ueshita, K., & Nonogaki, K. (1971). Classification of Coarse Soils Based on Engineering Properties. *Soils and Foundations*, *11*(3), 91–111. https://doi.org/10.3208/sandf1960.11.3_91

United Nations Office for Disaster Risk Reduction (UNDRR) & International Science Council (ISC). (2025, August 15). *UNDRR–ISC Hazard Information Profiles – 2025 Update: CH0100 Heavy Metals and Other Trace Elements United Nations Office for Disaster Risk Reduction*. International Science Council. https://www.preventionweb.net/understanding-disaster-risk/terminology/hips/ch0100

Ural, N. (2018). The Importance of Clay in Geotechnical Engineering. In *Current Topics in the Utilization of Clay in Industrial and Medical Applications*. InTech. https://doi.org/10.5772/intechopen.75817

Uy, S. (2021). Utilization of Philippine gold mine tailings as a material for geopolymerization. *International Journal of GEOMATE*, *21*(83). https://doi.org/10.21660/2021.83.9248

Veiga, M. M., Angeloci, G., Hitch, M., & Colon Velasquez-Lopez, P. (2014). Processing centres in artisanal gold mining. *Journal of Cleaner Production*, *64*, 535–544. https://doi.org/10.1016/j.jclepro.2013.08.015

Vriens, B., Plante, B., Seigneur, N., & Jamieson, H. (2020). Mine Waste Rock: Insights for Sustainable Hydrogeochemical Management. *Minerals*, *10*(9), 728. https://doi.org/10.3390/min10090728

Wentworth, C. K. (1922). A Scale of Grade and Class Terms for Clastic Sediments. *The Journal of Geology*, *30*(5), 377–392.

Wyszkowski, M., & Brodowska, M. S. (2020). Phytoextraction with Maize of Soil Contaminated with Copper after Application of Mineral and Organic Amendments. *Agronomy*, *10*(10), 1597. https://doi.org/10.3390/agronomy10101597

Yang, W., Lan, X., Wang, Q., Dong, P., & Wang, G. (2021). Selective pre-leaching of tellurium from telluride-type gold concentrate. *Frontiers in Chemistry*, *9*. https://doi.org/10.3389/fchem.2021.593888

Yotova, G., Padareva, M., Hristova, M., Astel, A., Georgieva, M., Dinev, N., & Tsakovski, S. (2018). Establishment of geochemical background and threshold values for 8 potential toxic elements in the Bulgarian soil quality monitoring network. *Science of The Total Environment*, *643*, 1297–1303. https://doi.org/10.1016/j.scitotenv.2018.06.237

Zhang, J., Zhang, Y., Richmond, W., & Wang, H. (2010). Processing technologies for gold-telluride ores. *International Journal of Minerals, Metallurgy, and Materials*, *17*(1), 1–10. https://doi.org/10.1007/s12613-010-0101-6

Zhao, B., O'Connor, D., Zhang, H., Jin, Y., Wang, Y., Yang, X., Hou, R., & Hou, D. (2023). Assessing mercury pollution at a primary ore site with both ancient and industrial mining and

smelting activities. *Environmental Pollution*, *336*, 122413. https://doi.org/10.1016/j.envpol.2023.122413

SUPPLEMENTARY INFORMATION

Table S1. C_u and C_c criteria for soil gradation based on geotechnical literature

Parameter	Interpretation	Reference
$C_u \approx 1$	Uniformly graded soil; particles are nearly the same size.	Ueshita & Nonogaki 1971; ASTM D2487
$C_u > 4$ and $1 \leq C_c \leq 3$	Well-graded gravel	Kalore & Sivakumar Babu 2023; Ueshita & Nonogaki 1971; ASTM D2487
$C_u > 6$ and $1 \leq C_c \leq 3$	Well-graded sand	Kalore & Sivakumar Babu 2023; Ueshita & Nonogaki 1971; ASTM D2487
$C_c < 1$ or $C_c > 3$	Poorly-graded or gap-graded soil	Kalore & Sivakumar Babu 2023; Ueshita & Nonogaki 1971; ASTM D2487

Table S2. ICP-MS detection limits, over-range values, and a comparison of expected and measured values for CRM.

Elements	Cu (mg/kg)	Pb (mg/kg)	Zn (mg/kg)	Ag (g/t)	As (mg/kg)	Sb (mg/kg)	Al (%)	Ca (%)	Cd (mg/kg)	Co (mg/kg)	Cr (mg/kg)	Fe (%)	K (%)	Mg (%)	Mn (mg/kg)
Detection Limit	0.5	0.5	1	0.05	0.5	0.05	0.005	0.005	0.02	0.1	1	0.01	0.002	0.002	1
Over Range	20,000	10,000	20,000	500	10000	10000	15	40	2000	10,000	20,000	50	10	40	20,000
Blank Run	<0.5	<0.5	<1	<0.05	<0.5	<0.05	<0.005	<0.005	<0.02	<0.1	<1	<0.01	<0.002	<0.002	<1
OREAS 44P															
Measured	444.9	224.9	624		105	15.64	3.905	0.328	0.1	61.5	1877	34.66	1.276	0.448	843
Expected	421	210	619	0.71	105	15	3.74	0.33	0.21	63	1838	34.51	1.24	0.48	830
OREAS 601d															
Measured	1,066.1	995.5	991		668.7	37.75	7.407	0.755	9.09	4.1	18	2.41	-	0.171	247
Expected	1067.8	986.4	973	48.73	683.3	40.72	7.132	0.738	9.7	4	18	2.39	-	0.168	250
OREAS 603b															
Measured	9,477.8	860	1,988		2,444.9	298.33	6.485	0.616	11.59	10	29	3.62	1.933	0.078	159
Expected	9,728.6	862	2,015	292.7	2,432.8	306.7	6.482	0.618	12.34	9.4	26	3.67	1.959	0.073	162
OREAS 624															
Measured	-	6,298.6	-	-	-	-	-	-	131.68	-	-	-	-	1.273	-
Expected	-	6240	-	-	-	-	-	-	132	-	-	-	-	1.26	-
OREAS90															
Measured	108.2	6.7	63		4.9	0.78	8.167	0.505	0.04	16	68	4.41	-	1.755	657
Expected	112	6.6	68	<0.05	4.5	0.88	8.36	0.48	0.02	15.3	82	4.76	-	1.9	663

Elements	Na (%)	Ni (mg/kg)	P (%)	Sc (mg/kg)	Ce (ppm)	Dy (ppm)	La (ppm)	Nd (ppm)	Te (ppm)	Ti (%)	Y (ppm)	U (ppm)	Th (ppm)
Detection Limit	0.002	0.5	0.005	0.1	0.01	0.01	0.01	0.01	0.05	0.0005	0.05	0.01	0.01
Over Range	10	20,000	5	5,000	10,000	2,000	5,000	2,000	2,000	2	2,000	10,000	5,000
Blank Run	<0.002	<0.5	<0.005	<0.1	<0.01	<0.01	<0.01	<0.01	<0.05	<0.0005	<0.05	<0.01	<0.01
OREAS 44P													
Measured	-	497.3	0.041	7.7	52.84	2.28	25.6	23.43	-	0.1641	13.04	3.7	8.37
Expected	-	460	0.04	8	50.83	2.27	23	23.69	-	0.166	11.5	3.58	8.33
OREAS 601d													
Measured	1.658	6.2	0.04	5	76.01	3.26	38.83	31.87	3.94	0.1809	13.29	4.36	11.13
Expected	1.63	7.2	0.039	4.9	74.17	3.1	37.63	31.86	4.58	0.1808	13.41	4.24	12.35
OREAS 603b													
Measured	1.344	-	0.036	3.9	46.05	1.84	22.2	19.16	39.74	0.1492	8.22	3.68	6.07
Expected	1.384	-	0.039	4.1	47.95	1.95	22.12	22.26	36.52	0.1495	8.57	3.82	8.87
OREAS 624													
Measured	-	-	-	-	-	-	-	-	-	-	-	-	-
Expected	-	-	-	-	-	-	-	-	-	-	-	-	-
OREAS90													
Measured	0.515	85.5	0.069	13.8	94.02	5.78	47.89	38.76	-	0.4155	28.36	3.44	17.53
Expected	0.52	92	0.07	13	92.9	5.67	48	39.35	-	0.41	29.52	3.32	18

Table S3. Computed I_{geo} and EF values in Paracale and Masbate samples. The median from n number of samples was used in the computation.

Sample Category	Pollution Indices/PTEs (in mg/kg)	THg	Cu	Pb	As	Cr	Cd	Sb	Zn	Ni	Co
Paracale tailings (n = 4)	I_{geo}	8.87	6.75	7.62	8.03	-0.44	9.63	8.72	6.67	0.49	-0.71
	EF	3,774.44	866.88	1,583.71	2,104.99	5.94	6,401.71	3,404.42	825.01	11.31	4.95
Paracale muck-outs (n = 2)	I_{geo}	3.12	6.91	7.44	7.52	0.07	8.99	12.08	5.99	-2.28	-3.02
	EF	215.20	2,976.29	4,289.33	4,526.67	25.87	12,525.88	10,6803.74	1,573.80	5.08	3.05

Masbate tailings	I_{geo}	3.30	1.60	2.57	4.16	-1.94	1.33	3.71	0.52	-2.09	-0.40
(n = 3)	EF	12.51	3.86	7.53	22.73	0.33	3.21	16.65	1.82	0.30	0.97
Masbate low-	I_{geo}	2.24	0.75	-0.68	6.07	-0.10	1.25	5.38	-0.22	-1.34	-1.06
grade ore (n = 2)	EF	8.41	3.00	1.11	119.58	1.66	4.22	73.97	1.53	0.70	0.85

Table S4. Sieve results for the Paracale and Masbate tailings.

PAR-01

Sieve No. (ASTM E11)	Opening (mm)	Sieve Wt. (g)	Sieve + Soil Wt. (g)	Wt. of soil retained (g)	% Retained	Cumulative % Retained	%Finer
5	4	473.63	473.83	0.2	0.04	0.04	99.96
10	2	470.42	476.85	6.43	1.29	1.33	98.67
18	1	415.98	430.83	14.85	2.97	4.29	95.71
35	0.5	354.85	411.74	56.89	11.37	15.67	84.33
60	0.25	353.12	389.21	36.09	7.22	22.88	77.12
120	0.125	337.61	432.49	94.88	18.97	41.85	58.15
170	0.09	306.26	376.35	70.09	14.01	55.87	44.13
230	0.063	329.47	501.7	172.23	34.43	90.30	9.70
Pan	-	368.67	417.13	48.46	9.69	99.99	0.01

PAR-02

Sieve No. (ASTM E11)	Opening (mm)	Sieve Wt. (g)	Sieve + Soil Wt. (g)	Wt. of soil retained (g)	% Retained	Cumulative % Retained	%Finer
5	4	473.67	473.84	0.17	0.03	0.03	99.97
10	2	470.6	471.93	1.33	0.27	0.30	99.70
18	1	416.1	421.86	5.76	1.15	1.45	98.55
35	0.5	355.66	374.49	18.83	3.76	5.22	94.78
60	0.25	353.67	437.88	84.21	16.84	22.05	77.95
120	0.125	338.72	516.92	178.2	35.63	57.68	42.32
170	0.09	307.32	402.03	94.71	18.94	76.62	23.38
230	0.063	329.52	396.72	67.2	13.44	90.06	9.94
Pan	-	368.95	416.76	47.81	9.56	99.62	0.38

PAR-03

Sieve No. (ASTM E11)	Opening (mm)	Sieve Wt. (g)	Sieve + Soil Wt. (g)	Wt. of soil retained (g)	% Retained	Cumulative % Retained	%Finer
5	4	473.67	473.71	0.04	0.01	0.01	99.99
10	2	470.4	470.64	0.24	0.05	0.06	99.94
18	1	415.9	417.15	1.25	0.25	0.31	99.69
35	0.5	354.83	357.21	2.38	0.48	0.78	99.22
60	0.25	352.99	370.61	17.62	3.52	4.30	95.70
120	0.125	337.4	501.65	164.25	32.84	37.15	62.85
170	0.09	306.74	489.31	182.57	36.51	73.65	26.35
230	0.063	329.39	411.17	81.78	16.35	90.00	10.00
Pan	-	368.75	417.77	49.02	9.80	99.81	0.19

PAR-05

Sieve No. (ASTM E11)	Opening (mm)	Sieve Wt. (g)	Sieve + Soil Wt. (g)	Wt. of soil retained (g)	% Retained	Cumulative % Retained	%Finer
5	4	473.61	476.17	2.56	0.51	0.51	99.49
10	2	470.42	477.36	6.94	1.39	1.90	98.10
18	1	415.91	424.45	8.54	1.71	3.61	96.39
35	0.5	354.81	369.85	15.04	3.01	6.61	93.39
60	0.25	353.01	377.46	24.45	4.89	11.50	88.50
120	0.125	336.16	453.56	117.4	23.47	34.97	65.03
170	0.09	306.22	405.94	99.72	19.93	54.90	45.10
230	0.063	329.36	410.72	81.36	16.26	71.16	28.84
Pan	-	368.63	512.45	143.82	28.75	99.91	0.09

MGP-01

Sieve No. (ASTM E11)	Opening (mm)	Sieve Wt. (g)	Sieve + Soil Wt. (g)	Wt. of soil retained (g)	% Retained	Cumulative % Retained	%Finer
5	4	473.73	473.83	0.1	0.04	0.04	99.96
10	2	470.76	474.55	3.79	1.37	1.41	98.59
18	1	416.61	421.5	4.89	1.77	3.18	96.82
35	0.5	355.49	389.26	33.77	12.24	15.42	84.58
60	0.25	353.23	385.72	32.49	11.78	27.20	72.80
120	0.125	337.46	414.5	77.04	27.93	55.13	44.87
170	0.09	306.8	352.31	45.51	16.50	71.62	28.38
230	0.063	329.39	377.72	48.33	17.52	89.14	10.86
Pan	-	368.86	397.43	28.57	10.36	99.50	0.50

MGP-02

Sieve No. (ASTM E11)	Opening (mm)	Sieve Wt. (g)	Sieve + Soil Wt. (g)	Wt. of soil retained (g)	% Retained	Cumulative % Retained	%Finer
5	4	476.08	479.66	3.58	0.72	0.72	99.28
10	2	472.67	488.9	16.23	3.25	3.96	96.04
18	1	417.51	425.6	8.09	1.62	5.58	94.42
35	0.5	356.54	388.93	32.39	6.48	12.06	87.94
60	0.25	353.56	458.38	104.82	20.96	33.02	66.98
120	0.125	336.66	536.78	200.12	40.02	73.04	26.96
170	0.09	307.54	362.02	54.48	10.89	83.93	16.07
230	0.063	330.04	367.64	37.6	7.52	91.45	8.55
Pan	-	369.82	410.18	40.36	8.07	99.52	0.48

MGP-03

Sieve No. (ASTM E11)	Opening (mm)	Sieve Wt. (g)	Sieve + Soil Wt. (g)	Wt. of soil retained (g)	% Retained	Cumulative % Retained	%Finer
5	4	473.6	473.62	0.02	0.0039988	0.0039988	100.00
10	2	470.47	470.52	0.05	0.009997	0.0139958	99.99
18	1	415.97	416.37	0.4	0.07997601	0.09397181	99.91
35	0.5	355.06	369.8	14.74	2.94711587	3.04108767	96.96
60	0.25	353.04	403.71	50.67	10.1309607	13.1720484	86.83
120	0.125	338.27	476.9	138.63	27.7176847	40.8897331	59.11
170	0.09	307.14	409.56	102.42	20.4778566	61.3675897	38.63
230	0.063	329.39	401.03	71.64	14.3237029	75.6912926	24.31
Pan	-	368.86	488.54	119.68	23.9288214	99.620114	0.38

Table S5. Descriptive statistics value (mean, standard deviation, median, and range) for the elements detected in Paracale and Masbate samples.

Sample Category	Descriptive Statistics	Au (g/t)	Ag (g/t)	Cu (%)	THg (ppm)	Pb (ppm)	Zn (ppm)	As (ppm)	Sb (ppm)	Cd (ppm)	Co (ppm)	Cr (ppm)	Ni (ppm)
Paracale tailings (n = 4)	Mean	8.37	115.47	0.52	42.64	3812.03	10029.75	2612.83	423.17	117.08	15.28	104.75	128.78
	StDev	4.46	139.13	0.42	35.21	2057.63	5587.91	2565.44	451.96	86.57	1.39	45.07	86.23
	Median	8.64	46.48	0.45	35.05	5000.00	10265.50	1876.45	252.90	107.00	15.90	101.50	98.70
	Range	12.56	341.54	1.14	96.71	4751.90	15782.00	6609.40	1175.29	236.59	3.50	98.00	228.30
Paracale muck-outs (n = 2)	Mean	1.65	127.11	0.51	0.65	4427.20	6402.00	1319.20	2593.81	68.45	3.20	144.50	14.50
	StDev	0.86	122.89	0.49	0.53	572.80	4787.00	1202.80	2582.23	59.40	1.10	8.50	9.10
	Median	1.65	127.11	0.51	0.65	4427.20	6402.00	1319.20	2593.81	68.45	3.20	144.50	14.50
	Range	1.71	245.78	0.99	1.06	1145.60	9574.00	2405.60	5164.45	118.79	2.20	17.00	18.20
Masbate tailings (n = 3)	Mean	0.21	0.77	0.01	0.68	160.67	137.67	123.20	7.71	0.36	19.83	38.00	17.60
	StDev	0.03	0.05	0.00	0.15	16.65	9.67	18.44	0.39	0.03	0.66	3.56	1.70
	Median	0.20	0.74	0.01	0.74	150.90	144.00	128.60	7.85	0.34	19.70	36.00	16.60
	Range	0.08	0.12	0.00	0.36	37.10	21.00	44.20	0.93	0.06	1.60	8.00	3.80
Masbate low-grade ore (n = 2)	Mean	1.22	3.21	0.01	0.35	15.90	86.50	483.80	24.94	0.32	12.45	128.50	27.80
	StDev	0.95	2.63	0.00	0.31	5.10	18.50	451.60	13.09	0.08	6.65	19.50	21.50
	Median	1.22	3.21	0.01	0.35	15.90	86.50	483.80	24.94	0.32	12.45	128.50	27.80
	Range	1.90	5.26	0.01	0.62	10.20	37.00	903.20	26.18	0.16	13.30	39.00	43.00

Sample Category	Descriptive Statistics	Sc (ppm)	Ce (ppm)	Dy (ppm)	La (ppm)	Nd (ppm)	P (%)	S (%)	Te (ppm)	Ti (%)	Y (ppm)	U (ppm)	Th (ppm)
Paracale tailings (n = 4)	Mean	3.03	16.35	1.10	7.83	8.16	0.03	4.43	29.01	0.06	5.47	2.54	0.87
	StDev	1.08	6.82	0.59	3.23	2.63	0.01	2.84	37.87	0.02	2.88	2.90	0.23
	Median	2.60	16.59	0.83	8.07	8.08	0.03	4.67	9.71	0.06	4.34	1.11	0.96
	Range	2.70	17.88	1.48	8.59	6.87	0.02	7.97	92.15	0.06	7.44	7.09	0.57
Paracale muck-outs (n = 2)	Mean	0.85	7.97	0.29	3.93	3.71	0.01	3.81	40.21	0.03	1.21	0.21	0.37
	StDev	0.15	2.45	0.03	1.21	0.99	0.00	1.19	39.33	0.00	0.08	0.08	0.14
	Median	0.85	7.97	0.29	3.93	3.71	0.01	3.81	40.21	0.03	1.21	0.21	0.37
	Range	0.30	4.90	0.06	2.41	1.98	0.00	2.38	78.66	0.01	0.15	0.16	0.28
Masbate tailings (n = 3)	Mean	16.43	18.51	2.31	9.00	10.48	0.15	1.30	0.76	0.29	11.96	0.66	1.28
	StDev	1.39	1.06	0.17	0.60	0.53	0.02	0.27	0.11	0.01	0.27	0.02	0.18
	Median	16.50	18.86	2.42	9.28	10.48	0.15	1.42	0.73	0.29	11.97	0.66	1.39
	Range	3.40	2.52	0.36	1.38	1.31	0.05	0.64	0.26	0.01	0.65	0.04	0.41
Masbate low-grade ore (n = 2)	Mean	11.80	12.78	1.41	6.48	7.43	0.21	2.44	0.58	0.16	7.47	0.45	0.74
	StDev	3.90	4.35	0.25	1.98	2.51	0.04	1.74	0.02	0.09	0.97	0.24	0.43
	Median	11.80	12.78	1.41	6.48	7.43	0.21	2.44	0.58	0.16	7.47	0.45	0.74
	Range	7.80	8.69	0.49	3.96	5.01	0.07	3.49	0.03	0.17	1.94	0.48	0.85

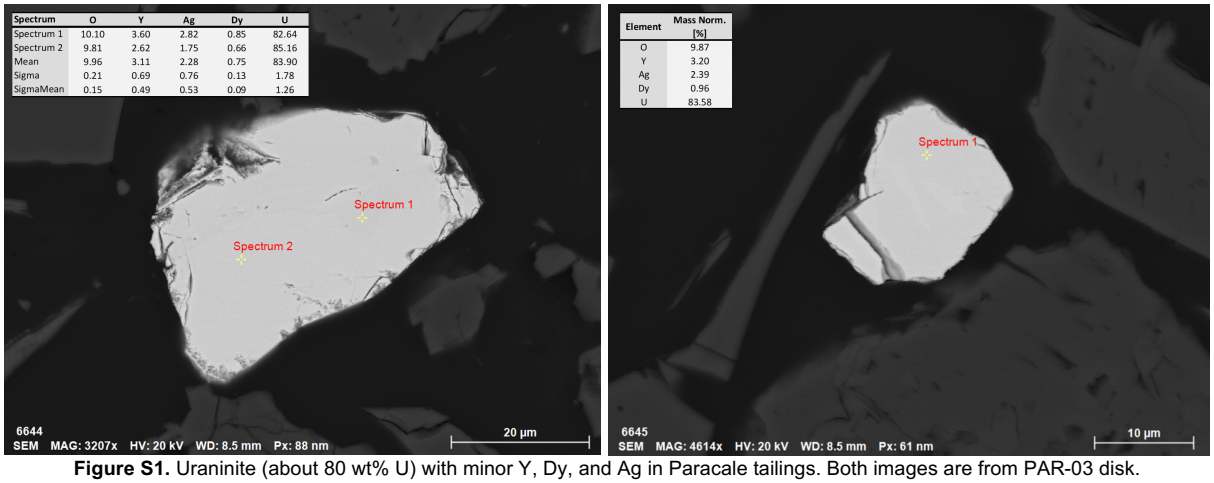


Figure S1. Uraninite (about 80 wt% U) with minor Y, Dy, and Ag in Paracale tailings. Both images are from PAR-03 disk.

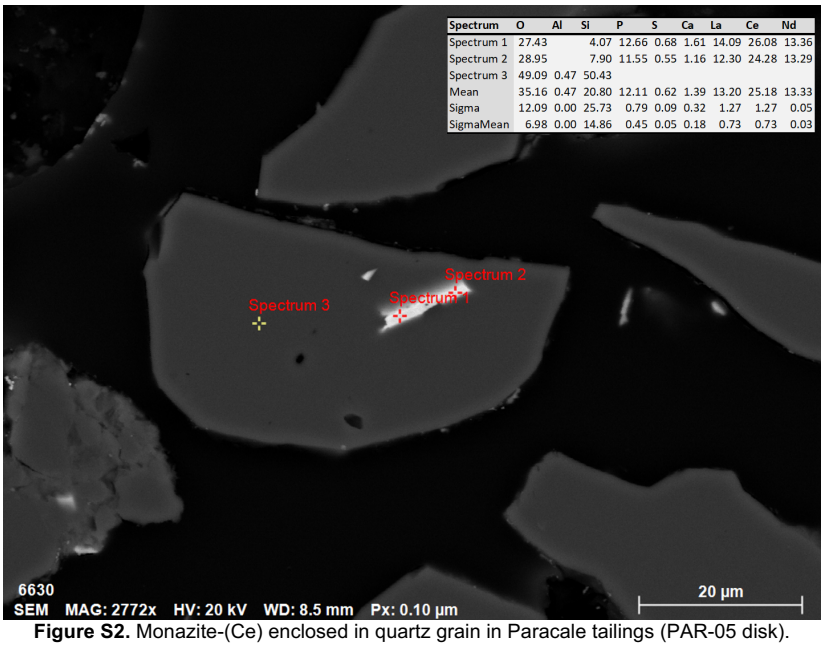


Figure S2. Monazite-(Ce) enclosed in quartz grain in Paracale tailings (PAR-05 disk).

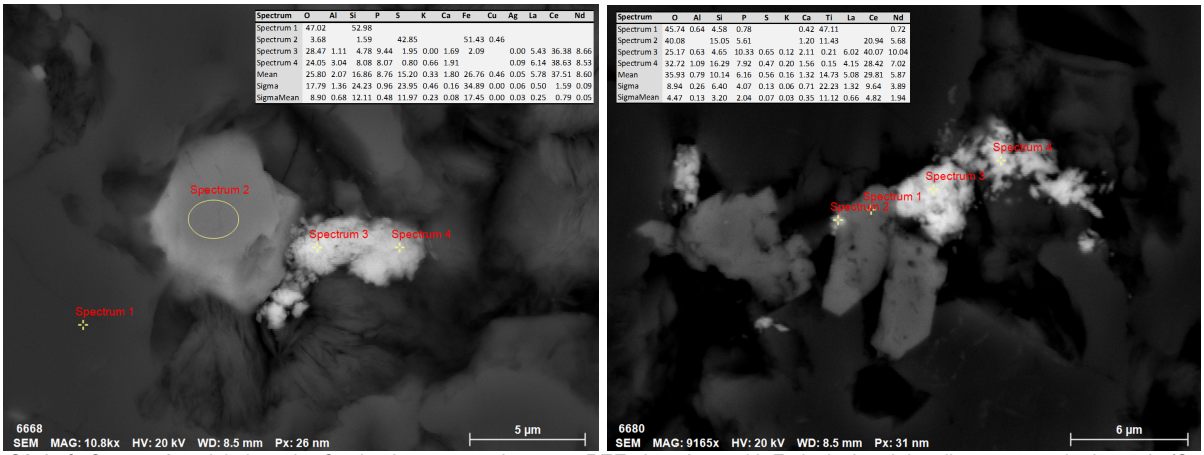


Figure S3. Left: Spectra 3 and 4 show the Ce-dominant monazite-group REE phosphate with Fe inclusion. It is adjacent to pyrrhotite grain (Spectrum 2). Both are enclosed in larger quartz grain. Right: Spectrum 1 is the REE-Ti phosphate while Spectra 2 to 4 are Ce-, Nd-, and La-bearing monazite. Both SEM images are from MGP-05 thin section.